Scientific Research Publishing

Open Journal of Inorganic Chemistry, 2021, 11, 145-175
https://www.scirp.org/journal/ojic
ISSN Online: 2161-7414
ISSN Print: 2161-7406

Structural, Theoretical and Biological Studies of (Z)-3-Amino-N-(3-Amino Pyrazine-2-Carbonyl) Pyrazine-2-Carbohydrazonic Acid (APA; L) and Its Cu^{2+}, Co^{2+}, Pt^{4+} and Pd^{2+} Chelates

Mosaad R. Mlahi[1], Mohsen M. Mostafa[2*]

[1]Faculty of Science, Department of Chemistry, Amran University, Amran, Yemen
[2]Faculty of Science, Department of Chemistry, Mansoura University, Mansoura, Egypt
Email: *amohsenmostafa@Yahoo.com

How to cite this paper: Mlahi, M.R. and Mostafa, M.M. (2021) Structural, Theoretical and Biological Studies of (Z)-3-Amino-N-(3-Amino Pyrazine-2-Carbonyl) Pyrazine-2-Carbohydrazonic Acid (APA; L) and Its Cu^{2+}, Co^{2+}, Pt^{4+} and Pd^{2+} Chelates. *Open Journal of Inorganic Chemistry*, **11**, 145-175.
https://doi.org/10.4236/ojic.2021.114010

Received: August 4, 2021
Accepted: October 24, 2021
Published: October 27, 2021

Abstract

New chelates derived from the novel ligand, (Z)-3-amino-N-(3-amino pyrazine-2-carbonyl)pyrazine-2-carbohydrazonic acid (**APA**, **L**), with Cu^{2+}, Co^{2+}, Pt^{4+} and Pd^{2+} salts were investigated. The results suggest that APA acts as mononegative tridentate in the case of Cu^{2+}, binegative tetradentate in the case of Co^{2+} and as mononegative bidentate towards Pt^{4+} and Pd^{2+} chelates. The results of the corrected $\mu_{eff.}$ and spectral suggest the structures of the isolated chelates. The results of the corrected $\mu_{eff.}$ and spectral suggest the geometries of the isolated chelates. Molecular modeling is deduced and chemical reactivity, energy components for chelates and also MEP for **APA** is illustrated. *In Vitro*, the SOD and radical scavengers like activity of the synthesized compounds Hep G2 liver cancer cells and cytotoxic activity were checked. Metal chelates show potent anti-oxidative activity. The results of cytotoxic activity assay against hepatocellular carcinoma cell line Hep G2 confirmed that Pt^{4+} complex has the highest value, while **APA**, Cu^{2+}, Co^{2+} and Pd^{2+} chelates have no significant cytotoxic activity.

Keywords

Aminopyrazine, Density Function Theory Calculations, Antioxidant and Cytotoxic Activity, Biological Studies

1. Introduction

Heterocyclic compounds containing nitrogen show multidirectional pharmacological activity like diuretic [1] [2], antitumor [3] [4] [5] [6] and hypotensive [7]

[8] [9]. On searching of the anticipated biologically active compounds, we had cared in 3-aminopyrazin-2-hydrazide [10]. The pyrazine derivatives are also utilized in many pharmaceuticals as well as the products used for plant protection [11] [12]. Our research devotes especially to the compounds having potential tuberculosis activity [10]. Pyrazinamide, as an example of pyrazine derivatives, is well known as an effective therapeutics in infections caused by *M. tuberculosis*. The pervasive incidence of simple pyrazine molecules in nature, especially in the flavors of many food systems, their effectiveness at very low concentrations as well as the still increasing applications of synthetic pyrazines in the flavor and fragrance industry are queried for the high interest in these compounds [13]. Specific pyrazines, especially dihydropyrazines, are essential for all forms of life due to their DNA strand breakage activity and/or by their influencing of apoptosis [14]. Synthetic pyrazine derivatives have also been advantageous as drugs (antiviral, anticancer, antimycobacterial, etc.) fungicides, and herbicides [15]. Furthermore, 3-amino-6-chloro-pyrazine-6-carboxylic acid, as an example of a simple pyrazine compound, has shown an anti-auxin behavior. The significance of the pyrazine (1,4-diazine) ring for the activity of the biological herbicides can be assessed primarily according to the size of the investigated molecules. In this work, the potent active antioxidant and cytotoxic activities of the separated chelates on HepG2 liver cancer cells have been examined. The structures of the resulting **APA** and its chelates have been achieved on the basis of elemental analyses, spectral (IR, UV-vis., ^{1}H-NMR, ^{13}C-NMR mass), magnetic and thermal measurements and supported by Density Functional Theory (DFT) method.

The goal of our work is to check in detail the chelation behavior of the novel (Z)-3-amino-N-(3-aminopyrazine-2-carbonyl) pyrazine-2-carbohydrazonic acid (**APA**) and its chelates derived from Cu^{2+}, Co^{2+}, Pt^{4+} and Pd^{2+} ions, embedding structural articulation and molecular modeling of both **APA** and its chelates. Moreover, our attention is directed to evaluate the antioxidant and anticancer activity of the ligand as well as the detached chelates.

2. Experimental

2.1. Materials

All the chemicals are of AR quality and used as supplied. Elemental analyses (C, H, N), chloride and metal contents were determined by conventional methods [16]. Spectral and TGA studies were carried as reported in our previous work [17] [18]. Also, all the chemicals used in biological activity were reported earlier [18]. The diamagnetic corrections were determined using Pascal's constants [19].

2.2. Synthesis of the Ligand (APA) and Its Complexes

2.2.1. Synthesis of (Z)-3-amino-N-(3-aminopyrazine-2-carbonyl) pyrazine-2-carbo-hydrazonic Acid (APA)

The novel organic compound, (Z)-3-amino-N-(3-aminopyrazine-2-carbonyl) pyrazine-2-carbohydrazonic acid (**Figure 1(a)**, **Figure 1(b)**), was synthesized by adding slowly drop by drop of methyl 3-aminopyrazine-2-carboxylaste (1.53 g, 0.01

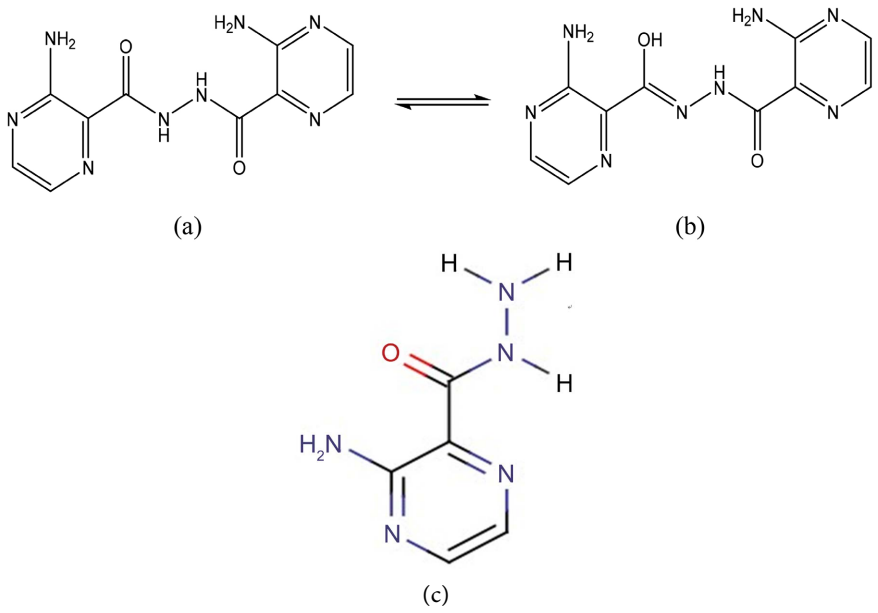

Figure 1. (Z)-3-amino-N-(3-aminopyrazine-2-carbonyl) pyrazine-2-carbohydrazonic acid (**APA**) in the keto (a) and enol (b) forms. (c) Structure of 3-amino-pyrazin-2-carbohydrazide.

mol) in absolute ethanol to N_2H_4 (8 mL). A pale yellow solid of **APA** was obtained by continuous stirring of the reaction mixture on a heater at 60˚C for 1.5 h. Doubtless the addition of methyl 3-aminopyrazine-2-carboxylate to excess hydrazine hydrate assists of the formation of **APA** and excludes the formation of 3-amino-pyrazin-2-carbohydrazide (**Figure 1(c)**). The novel product was obtained and collected by filtration followed by continuous washing several times with hot EtOH and ether. The isolated product was kept in a drier over anhydrous phosphorous pentaoxide. **APA** was recrystallized from absolute EtOH (Yield: 60%). The purity of **APA** was checked by spectral, TLC and its melting point (159˚C - 160˚C).

2.2.2. Synthesis of Cu^{2+}, Co^{2+}, Pt^{4+} and Pd^{2+} Chelates

Metal chelates were acquired by reacting 0.001 mol of **APA** (0.274 g, 0.001 mol) to metal chlorides ($CuCl_2{\cdot}2H_2O$; 0.17 g, $CoCl_2{\cdot}6H_2O$; 0.24 g, $PtCl_4$; 0.34 g; $PdCl_2$; 0.18 g) in 1:1 M ratio. The pH of the solution was optimized at 2, 3, 2 and 5, respectively. The isolated metal chelates with the general formulae, $C_{10}H_{13}Cu_2N_8O_4Cl_3$, $C_{12}H_{18}Co_2N_8O_5Cl_2$, $C_{14}H_{25}PtN_8O_6Cl_3$ and $C_{11}H_{14}PdN_8O_{7/2}Cl$, were isolated by filtration, rinsed continuously with EtOH and ether. The products were kept in a drier over P_4O_{10}. All the chelates are freely soluble in polar solvents and quite stable in air.

2.3. Biological Studies

2.3.1. Superoxide Dismutase Scavenging Activity

Both the metal chelates and **APA** were assessed against antioxidant activity [20]. The italicize of the ligand or its chelates to damped phenazine methosulphatemediated reduction of nitro blue tetrazolium dye was obtained from the results of

the assay. The determination of SOD was calculated as reported earlier [18].

2.3.2. Cell Cultures and Viability against HepG2

The safety of HepG2 cells in culture was carried out in triplicate and calculated by the MTT assay as reported in our earlier work [21].

2.4. Computational Details

DMOL^3 program [22] in materials studio package [23] was acquired for the data which is resolved for large-scale DFT calculations. DFT semi core pseudopods calculations were elicited with double numerical basis sets in addition to polarization functional. DNP basis sets are of comparable quality to 6-31G Gaussian basis sets [24]. The data acquired by DNP basis sets are more accurate than Gaussian basis sets of the same size as reported by Delley *et al.* [22]. The RPBE functional [25] is considered the best exchange-correlation function [26] establish on the generalized descended approximation (GGA) and is used to take account of the exchange and correlation impacts of electrons. Hence the geometric optimization is officiated without any symmetry curb.

3. Results and Discussion

Table 1 summarized the elemental analyses (C, H, M, and Cl) of the isolated metal chelates and some physical properties. The empirical formulae of the chelates are rimmed by elemental analyses (C, H, N, M, Cl) and confirmed by thermal gravimetric data. The low values of molar conductance (8 - 13 $ohm^{-1}\cdot cm^2\cdot mol^{-1}$ range) of the chelates in DMSO (Table 1) suggest their non-electrolytic nature [27]. Doubtless, the lower pH of the solution during complex formation (pH = 2, 3, 2 and 5 for Cu^{2+}, Co^{2+}, Pt^{4+} and Pd^{2+}, respectively) causes the block of the NH_2 groups and consequently the enolization of the carbonyl group occurred with the liberation of a proton during complex formation. Hence, all the compounds were obtained by losing one or two protons as shown in Table 1. The results

Table 1. Analytical and physical data of **APA** and its metal chelates.

Compound; (empirical formula)	(F. Wt)	Color	M.p. (˚C)	% Found (Calcd.)				A_m^+ (DMSO)	Yield (%)
				C	H	M	Cl		
APA; $C_{10}H_{10}N_8O_2$	274.246	Yellow	156 - 157	44.6 (43.8)	4.6 (3.7)	---	---	---	70
$[Cu_2(\mathbf{APA}\text{-}H)(H_2O)Cl_3]\cdot H_2O$; $C_{10}H_{13}Cu_2N_8O_4Cl_3$	542.721	Brown	> 300	22.9 (22.1)	3.1 (2.4)	23.1 (23.4)	20.0 (19.6)	9	83
$[Co_2(\mathbf{APA}\text{-}2H)(H_2O)_2Cl_2]\cdot EtOH$; $C_{12}H_{18}Co_2N_8O_5Cl_2$	543.098	Olive-green	> 300	26.01 (26.5)	4.2 (3.3)	20.96 (21.7)	13.7 (13.1)	10	76
$[Pt(\mathbf{APA}\text{-}H)(H_2O)Cl_3]\cdot H_2O\cdot 2EtOH$; $C_{14}H_{25}PtN_8O_6Cl_3$	702.849	Light-brown	> 300	23.2 (23.9)	4.1 (3.2)	----	16 (15.1)	13	90
$[Pd(\mathbf{APA}\text{-}H)(H_2O)C]\cdot 2/1EtOH$; $C_{11}H_{14}PdN_{8}O_{7/2}Cl$	456.162	Olive-green	> 300	29.6 (28.9)	3.3 (3.1)	23.5 (23.3)	8.5 (7.8)	8	69

suggest that the comparatively high pH values of the Co^{2+} and Pd^{2+} (pH = 3 and 5) complexes up stay for the liberations of two protons while the decline pH of Cu^{2+} and Pt^{4+} complexes give the chance to lose only one electron during the formation of the reactants.

3.1. IR Spectra

Two tautomer shapes [keto (a) and enol (b)] as elucidated in **Figure 1(a)**, **Figure 1(b)** are suggested for **APA** on the basis of the results of IR spectra. The infrared spectrum of **APA** (KBr) shows three bands at 3416, 3306 and 3200 cm^{-1} imputable to ν(OH), $\nu_a(NH_2)$ and $\nu_s(NH_2)$ [28] vibrations, respectively. The band at 3150 cm^{-1} is attributed to $\nu(NH_2)$ vibration [29]. The possibility of keto/enol tautomers (HN-C=O/N=C-OH) is reinforced by the observation of two NH group bands. The ν(C=O), $\nu(C=N)_{azom}$. And ν(C=N) vibrations of the pyrazine ring are observed at 1695, 1643 and 1562 cm^{-1}, respectively [30] [31]. All these basics were ascertained and supported by studding the modeling of the ligand as shown in **Figure 2**.

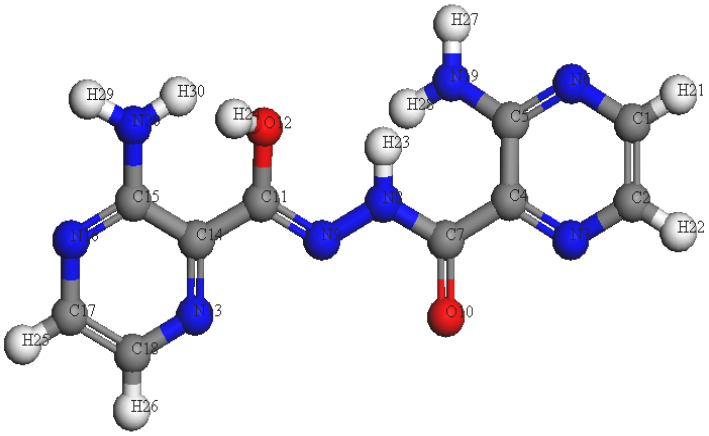

(a)

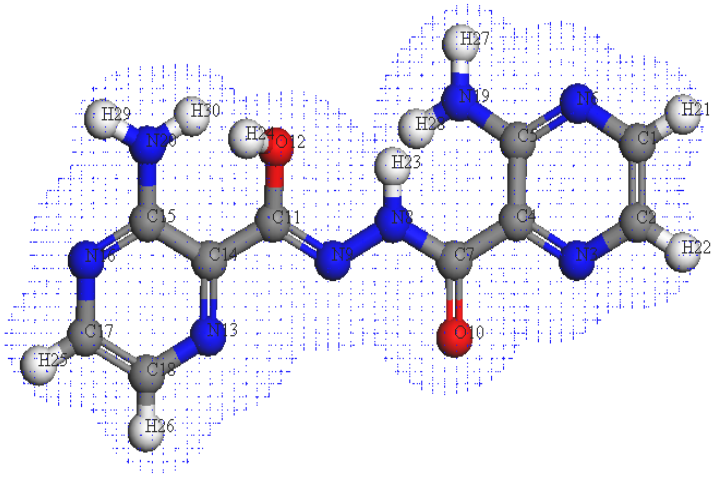

(b)

Figure 2. Molecular modeling of (a) **APA** (b) electron density.

The infrared spectra of **APA** and the isolated metal chelates (Table 2) show that the ligand binds to Cu^{2+} and Co^{2+} metal ions in 2:1 (M:L) ratio and 1:1 in case of Pt^{4+} and Pd^{2+} metal ions. **APA** behaves as mononegative tetradentate coordinating via the two nitrogen of NH_2 groups and two oxygen atoms with losing only one proton from the OH group (Figure 3) in case of $C_{10}H_{13}Cu_2N_8O_4Cl_3$. The bonding sites are revealed by: 1) the NH_2 and C=O groups are relocated to lower wavenumbers indicating that these groups are participate in chelation; 2) the observation of new band at 1331 cm^{-1} attributed to (C-O) group; 3) new bands are traced at 532 and 467 cm^{-1} assigned to M-O and M-N, respectively [32]. The spectrum of copper(II) chelate exhibits a broad band at 3416 cm^{-1} attributable to the water of coordination and water of solvation [33]. **APA** coordinates in a binegative tetradentate ligand via two NH_2 groups and two oxygen atoms with losing two protons from the two OH groups in case of Co^{2+}, with the general formulae, $C_{12}H_{18}Co_2N_8O_5Cl_2$ (Figure 4). This conduct revealed by:

1) The hiding of the (CO) group indicates this group is taking part in coordination after deprotonation.

2) The bands at 3285 - 3262 cm^{-1} attributable to (NH_2) are observed at lower wave numbers indicating that this group participates in bonding.

Table 2. The most important IR bands of **APA** and its metal chelates.

Compound	ν(OH)	ν(NH_2)	ν(NH)	ν(C=O)	ν(C=N)$_{azo}$	ν(C=N)$_{pyrz}$	ν(C-O)	ν(M-O)	ν(M-N)
APA; $C_{10}H_{10}N_8O_2$	3451	$(3381)_{as}$ $(3313)_s$	3187 3152	1695	1643	1562	----	----	----
$C_{10}H_{13}Cu_2N_8O_4Cl_3$	3416	$(3306)_{as}$ $(3197)_s$	3150	1686	1650	1556	1331	532	467
$C_{12}H_{18}Co_2N_8O_5Cl_2$	3401	$(3285)_{as}$ $(3262)_s$	----	----	1652 1616	1556	1335 1315	536	464
$C_{14}H_{25}PtN_8O_6Cl_3$	3405	$(3312)_F$ $(3293)_{Ch}$	3150	1711	1614	1562	1317	544	473
$C_{11}H_{14}PdN_8O_{7/2}Cl$	3422	$(3326)_F$ $(3309)_{Ch}$	3145	1708	1622	1569	1323	494	461

Note: azo: azomethine; pyrz: pyrazine ring.

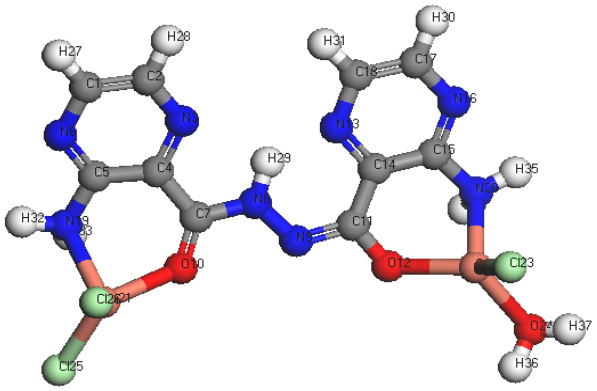

Figure 3. Molecular airing of $C_{10}H_{13}Cu_2N_8O_4Cl_3$.

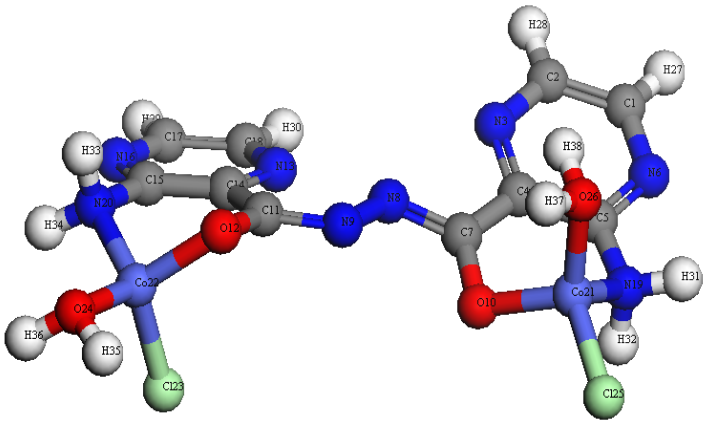

Figure 4. Molecular airing of $C_{12}H_{18}Co_2N_8O_5Cl_2$.

3) The NH band is obscured with the simultaneous observation of a new band in the 1652 - 1616 cm^{-1} region assigned to the $(C=N)_{azom}$, groups confirming the enolization of the NH groups together with the dislocation of a hydrogen atom from both OH groups.

4) Nouveau bands attributed to the (C-O) group are noticed in the 1553 - 1315 cm^{-1} regions.

5) Nouveau bands at 536 and 464 cm^{-1} are attributed to M-O and M-N [32].

6) The chelates exhibit a broad band at 3401 cm^{-1} assignable to H_2O and EtOH [33].

In the complexes, $C_{14}H_{25}PtN_8O_6Cl_3$ and $C_{11}H_{14}PdN_8O_{7/2}Cl$ (**Figure 5**, **Figure 6**), **APA** coordinates as a mononegative bidentate ligand through (N) of NH_2 group and (O) atom of deprotonated C-OH group. The chelation is suggested by the displacement of the NH_2 group to lower wavenumber together with the observation of new bands in the scale 1317 - 1323 cm^{-1} assigned to ν(C-O) vibration. The medium broad band at 3405 and 3422 cm^{-1} are assigned to the coordinated water as well as ethanol [33]. Also, the bands observed in the range 544 - 494 and 473 - 461 cm^{-1} are assigned to M-O and M-N, respectively [32].

3.2. Nuclear Magnetic Resonance Spectra (^{1}H-NMR and ^{13}C-NMR)

Three signals at 9.8, 7.5 and 4.5 ppm, relative to TMS, are observed in the ^{1}H-NMR spectrum of **APA** in d_6-DMSO (**Figure S1**) and attributed to the protons of OH [34], NH and NH_2 [28] groups and obscured on adding D_2O (**Figure S2**). The protons of pyrazine ring are noticed in the (7.7 - 8.3) region ppm. The observation of the OH signal suggests that **APA** is existed in the keto/enol forms as illustrated in **Figure 7**. Additional backing for the composition of the ligand is attested from the arising of ten signals in the ^{13}C-NMR spectrum (**Figure 1**) and the chemical shift of carbon (C=O) is observed at 167.02 ppm [35]. The signals assigned to C1, C2, C4 and C5 are noticed at 155.3, 133.0, 123.7 and 156.4 ppm, respectively. The existences of (OH) group adduced a great downfield shift of the (C14 and C18) and the up field shifts of C11 and C15 in accord with the

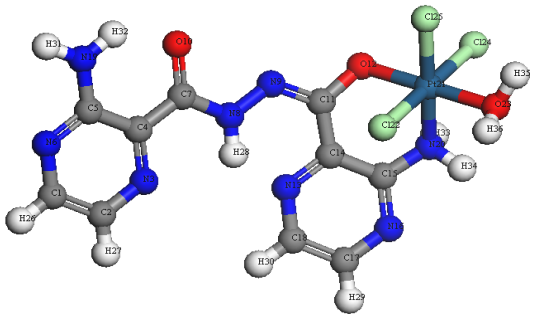

Figure 5. Molecular airing of $C_{14}H_{25}PtN_8O_6Cl_3$.

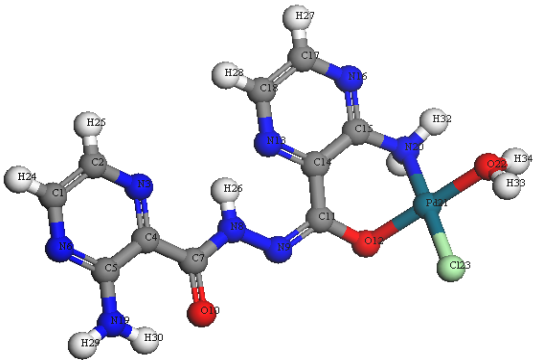

Figure 6. Molecular airing of $C_{11}H_{14}PdN_8O_{7/2}Cl$.

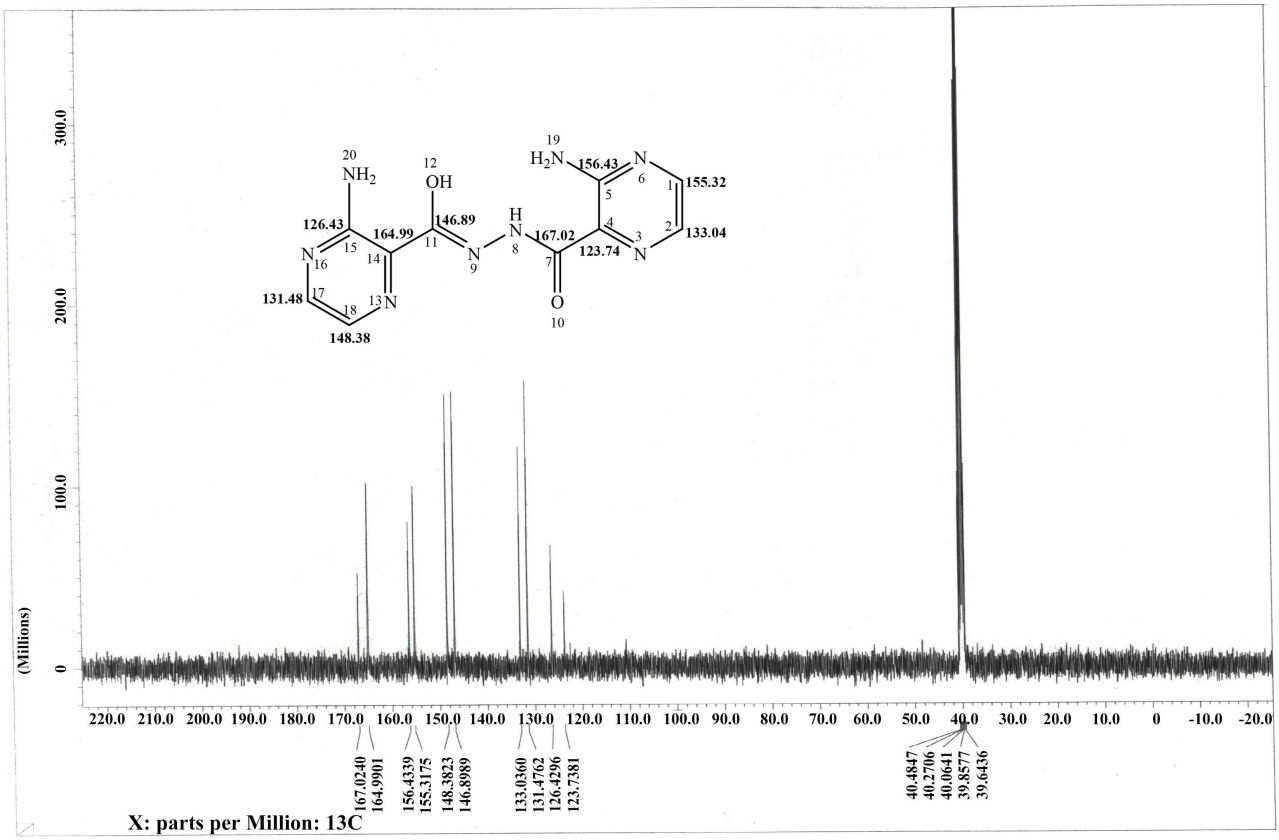

Figure 7. ^{13}C-NMR spectrum of **APA** in d_6-DMSO.

trend of π-electron densities [36], which is taken as a strong guide that **APA** is existed in the keto/enol forms.

The ^{1}H-NMR spectrum of Pt^{4+} chelate (**Figure S3**) shows signals at 9.01, 3.93 and 3.56 ppm attributed to NH, NH_2 and OH (EtOH and H_2O) protons, respectively. The protons of pyrazine ring are noticed in the 8.55 - 7.96 ppm range. The protons signal of ethanol (CH_3 and CH_2) are observed at 1.35 and 4.38 ppm indicating the existence of EtOH outside the coordination sphere [37]. The Pd^{2+} chelate spectrum (**Figure S4**) exhibits three signals at 8.27, 3.85 and 3.89 ppm assigned to NH, NH_2 and OH (EtOH and H_2O) protons, respectively. The protons of the pyrazine ring are traced in the 7.98 - 7.59 ppm range. The monitor of the proton signals of CH_3 and CH_2 (EtOH) outside the coordination sphere at 1.05 and 3.45 ppm verify the proposed formula [37].

3.3. Mass Spectra

Molecular ion peak noticed at m/z = 274 (10%) corresponds to ($C_{10}H_{10}N_8O_2$), M. wt. = 274.246, as shown in the mass spectrum of **APA** (**Figure 8**). Elemental analyses and spectral are taken as strong brochure for the suggested geometry.

APA ($C_{10}H_{10}N_8O_2$) fragmentation pattern shows successive segments. The peak at m/z 274.9 (10% abundance) represents the molecular ion (Calcd. 274.25). Also, the peak at 242 (46% abundance) symbolizs to $[C_{10}H_6N_6O_2]^{+\cdot}$ (Calcd. 242.2) and the peak in 224 (48% abundance) symbolizes to the fragment $[C_{10}H_4N_6O]^{+\cdot}$ (Calcd. 224.2). The peak at 135 (100% abundance) represents to $[C_5H_2N_4O]^{+\cdot}$ (Calcd. 134.1) portions. The peak in 102 with 46% abundance corresponds to $[C_5H_2N_2O]^{+\cdot}$ (Calcd. 106.1). The molecular ion peaks in the mass spectrum of $C_{12}H_{18}Co_2N_8O_5Cl_2$ approves with its formula. The mass spectrum of the Co^{2+} complex (**Figure S5**) elucidates the fragmentation example of the successive degradation of the chelate. The first peak at m/z 543.2 (0.02% abundance) represents the molecular ion (Calcd. 543.098). The peaks at 413, 299, 255, 199, 183, 153,

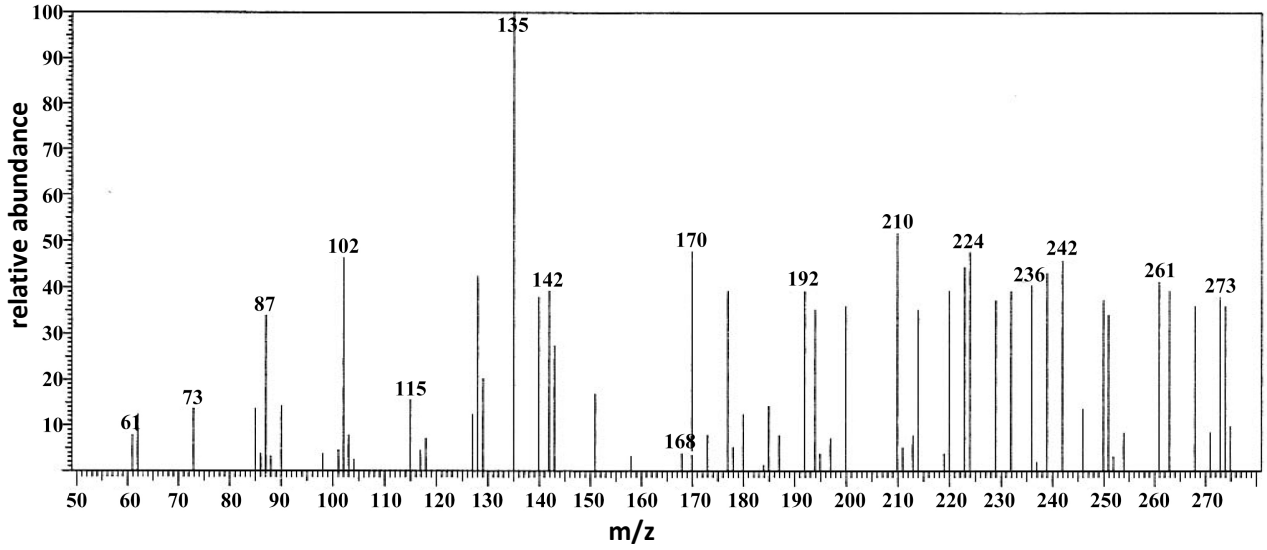

Figure 8. Mass spectrum of **APA**.

96, 77 and 51 with 2, 23, 10, 24, 15, 53, 89, 46 and 100% abundance (Calcd. 413.548, 301.149, 255.079, 199.054, 181.038, 153.027, 94.097, 78.074 and 51.048) correspond to $[C_8H_{14}Co_2N_5O_5Cl]^{+\cdot}$, $[C_8H_{12}CoN_5O_4]^{+\cdot}$, $[C_6H_6CoN_5O_3]^{+\cdot}$, $[C_5H_6CoN_3O_2]^{+\cdot}$, $[C_5H_4CoN_3O]^{+\cdot}$, $[C_4H_4CoN_3]^{+\cdot}$, $[C_4H_4N_3]^{+\cdot}$, $[C_4H_2N_2]^{+\cdot}$ and $[C_3HN]^{+\cdot}$ parts, respectively. Also, the mass spectrum of $C_{14}H_{25}PtN_8O_6Cl_3$ (**Figure S6**) shows a molecular ion peak at 702.6 which coincides with the theoretical value (702.849). The segment path of $C_{14}H_{25}PtN_8O_6Cl_3$ is illustrated in **Scheme S1**. $C_{11}H_{14}PdN_8O_{7/2}Cl$ (**Figure S7**) exhibits a molecular ion peak equals 456 which is agreed with the calculated value (456.162) as illustrated from the mass spectrum. **Scheme S2** depicts peaks corresponding to the successive degradation of Pd^{2+} chelate.

3.4. Spectral and Magnetic Results

All the electronic spectra of **APA** and its chelates were arises in Nujol mull. The chelates are distinctive by intense charge-transfer bands. The absorption band at 300 - 344 nm (33,333 - 28,901 cm^{-1}) is raised to $\pi \rightarrow \pi^*$ transition of pyrazine rings are shown in the spectrum of **APA**. The absorption band observed at 402 nm (24,815 cm^{-1}) is assigned to $n \rightarrow \pi^*$ of the NH_2 group, which shifts in chelates toward lower frequencies, supporting the chelation of the NH_2 group in bonding. Another two bands appear at 452 and 548 nm (22,123 and 18,284 cm^{-1}) are assigned to $\pi \rightarrow \pi^*$ of $(C=N)_{azom}$ and $n \rightarrow \pi^*$ transitions of the carbonyl group, respectively [38] [39]. The $^2B_2 \rightarrow {}^2E$ and $^2B_2 \rightarrow {}^2B_1$ transitions at 728 and 574 nm (13,736 and 17,421 cm^{-1}) in the electronic spectrum of the Cu^{2+} chelate (Nujol) confirms the presence of tetrahedral structure around the Cu^{2+} ion [40]. The band at 525 nm (19,047 cm^{-1}) is attributed to type $L \rightarrow M$ transition. The corrected magnetic moment value (μ_{eff} = 1.6 BM) is calculated for each Cu^{2+} ion [41]. Also, the Co^{2+} chelate shows three bands at 691, 562 and 418 nm (14,471, 17,793 and 23,923 cm^{-1}). The first two bands are assigned to $^4A_2 \rightarrow {}^4T_1$ (F) and $^4A_2 \rightarrow {}^4T_1$ (P) transitions in a tetrahedral geometry around the Co^{2+} ion. The band at 23,923 cm^{-1} is raised to charge-transfer ($L \rightarrow M$) [42]. The corrected magnetic moment (μ_{eff} = 4.4 BM) of Co^{2+} ion supports a tetrahedral geometry around the Co^{2+} [43]. The values of to be 10 Dq, B and β (519.9 cm^{-1}, 736.1 and 0.76), were calculated. Pt^{4+} chelate exhibits two bands at 486 and 440 nm (20,576 and 22,727 cm^{-1}) refers to the d-d transition bands $^1A_{1g} \rightarrow {}^1T_{1g}$ and $^1A_{1g} \rightarrow {}^1T_{2g}$, respectively [17]. Two bands at 388 and 592 nm (25,773 and 16,891 cm^{-1}) assigned to $^1A_{1g} \rightarrow {}^1B_{1g}$ and $^1A_{1g} \rightarrow {}^1E_g$ transitions in a square-planar configuration for the diamagnetic $C_{11}H_{14}PdN_8O_{7/2}Cl$ [17] [44].

3.5. Molecular Modeling

3.5.1. DFT Calculations for Optimization of the Geometry

The optimization of **APA** and its metal chelates are displayed in **Figures 2-6**. The bond lengths and angles calculated by optimized molecular geometry are given in **Tables S1-S10**. The important points are summarized as follow:

1) On chelation the bond angles of **APA** are shifted; the most important effective changes are shown in C(15)-N(20)-C(14), C(14)-C(11)-O(12), O(12)-C(11)-

N(9), O(10)-C(7)-C(4), N(19)-C(5)-C(4) and N(8)-C(7)-O(10), which are affected (decrease or increase) on chelation due to chemical bonding [45].

2) Tetrahedral geometry of the Cu(II) and Co(II) chelates, $C_{10}H_{13}Cu_2N_8O_4Cl_3$ and $C_{12}H_{18}Co_2N_8O_5Cl_2$, is proposed on the basis of the values of bond angles, while octahedral geometry is propounded for $C_{14}H_{25}PtN_8O_6Cl_3$, 2EtOH and a square-planar for $C_{11}H_{14}PdN_8O_{7/2}Cl$.

3) The metal chelates of **APA** are arraying according to M-O bond length as follows: O-Cu > O-Pt > O-Pd > O-Co.

4) According to M-N bond lengths the chelates of **APA** are arranged as follows: N-Cu > N-Pt > N-Pd > N-Co.

5) The angles around the metal centers undergo significant variations on changing the metal center while the bond angles in **APA** backbone do not change significantly.

3.5.2. Chemical Reactivity

1) Methods of Describing the Global Reactivity

The most important parameters in quantum calculations depend mainly on both the energies of the HOMO (π-donor) and LUMO (π-acceptor). These parameters are essentially behaved as an electron donor and electron acceptor, respectively, and these orbitals are known as Frontier Molecular Orbitals (FMOs).

1) The negative values of E_{HOMO} and E_{LUMO} and their neighboring orbitals (**Table 3**) anticipate the stability of the synthesized molecules [18].

2) The coordination sites (electrophilic attack) on aromatic compounds are easily anticipated using FMOs theory. The uttermost overlap between the HOMO on one molecule and the LUMO on the other illustrates that the reaction takes place. The most important factor in any reaction depends essentially on the interaction between HOMO and LUMO. The goal of the computations is to find out the highest values of molecular orbital coefficients. Consequently, the elevated value of molecular orbital coefficients for the ligand orbitals indicates its activity for chelation. All these keynotes are deduced from the data obtained

Table 3. Calculated E_{HOMO}, E_{LUMO}, energy band gap ($E_H - E_L$), chemical potential (μ), electronegativity (χ), global hardness (η), global softness (S), global electrophilicity index (ω) and softness (σ) for **APA** and its complexes.

Compound	E_H eV	E_L Ev	$(E_H - E_L)$ eV	χ eV	μ eV	H Ev	S eV^{-1}	Ω eV	σ eV
APA	−5.027	−2.493	−2.534	3.76	−3.76	1.267	0.6335	8.95617	0.789266
Cu complex	−5.199	−3.265	−1.934	4.232	−4.232	0.967	0.4835	8.6594	1.034126
Co complex	−4.485	−3.632	−0.853	4.0585	−4.0585	0.4265	0.21325	3.512531	2.344666
Pt complex	−5.516	−4.034	−1.482	4.775	−4.775	0.741	0.3705	8.447632	1.349528
Pd complex	−4.909	−3.462	−1.447	4.1855	−4.1855	0.7235	0.36175	6.337285	1.38217

H = HOMO, L = LUMO.

from calculations indicating that the nitrogen of NH_2 groups, oxygen of deprotonated C-OH and carbonyl groups with largest values of molecular orbital coefficients.

3) Linert *et al.* [45] showed that the bond strength increases as the adjacent bonds become weaker according to Guttmann's variation rules. This view agrees with the results of increasing of the value of E_{HOMO} accompanying by elongation followed by the weakness of the metal-ligand bonds and the narrowness of the positions abutted to the metal-ligand centers and thus becomes quite strong.

4) The level of HOMO is essentially domestic on the N(20), N(19) and O(10) and O(12) atoms (**Figure 9**) suggesting that these atoms are the most active nucleophile sites on the central metal ion. This indicates that these centers have high values of HOMO density coefficients and in face of the metal ions.

5) The energy gap (E_{HOMO}-E_{LUMO}) [45] is used to calculate the kinetic stability and chemical reactivity of the **APA**. The theoretical model for illustrating the geometry and approval barriers in different modulate, which governs the biological bustle of the molecule, depends mainly on the energy gap. The softness of the molecule (more polarized) is known from the small gap. Accordingly, the reactivity of soft molecules than hard ones is mainly due to the easily offer electrons to an acceptor. The charge-transfer is easily occurred due to the small energy gap in case of **APA** suggests which effectuating the biological activity of the molecule. The groups that enter into conjugation causes the low value of energy gap.

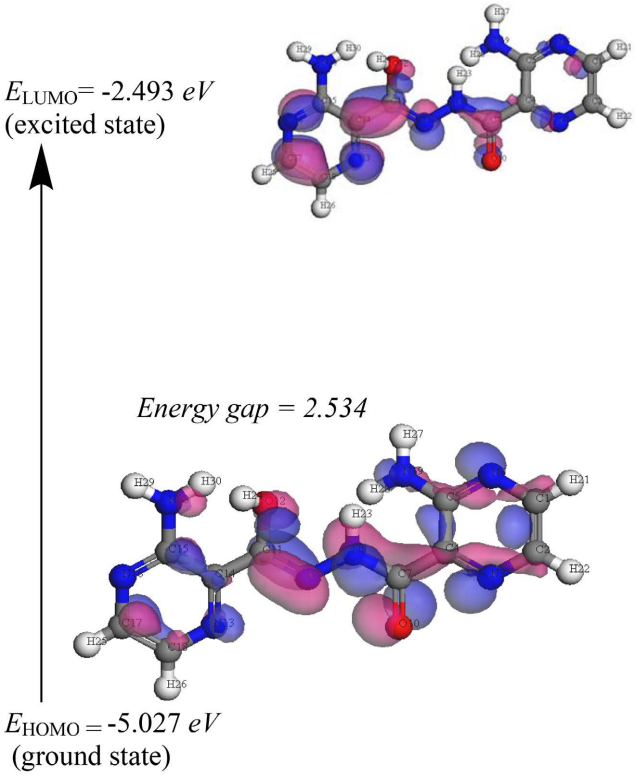

Figure 9. 3D plots frontier orbital energies using DFT method for **APA**.

6) The donating electron capacity is weaker due to the lowering of the HOMO energy values. Contrarily, the molecule becomes good electron donor when the HOMO energy becomes higher. The ability of a molecule to receive electron depends on the LUMO energy [45].

Both the site selectivity and chemical reactivity of the molecular systems is figured out from DFT. The energies of both ($E_{HOMO} + E_{LUMO}$) and ($E_{HOMO} - E_{LUMO}$) construe the charge-transfer interaction, electronegativity (χ), chemical potential (μ), global hardness (η), global softness (S) and global electrophilicity index (ω) within the molecule [46] [47]. The results are depicted in **Table 3**.

$$\chi = -1/2\left(E_{LUMO} + E_{HOMO}\right) \tag{1}$$

$$\mu = -\chi = 1/2\left(E_{LUMO} + E_{HOMO}\right) \tag{2}$$

$$\eta = 1/2\left(E_{LUMO} - E_{HOMO}\right) \tag{3}$$

$$S = 1/2\eta \tag{4}$$

$$\omega = \mu^2/2\eta \tag{5}$$

The inverse value of the global hardness bestowed the softness (σ) as follow:

$$\sigma = 1/\eta \tag{6}$$

The electrophilicity index is considered the most important quantum chemical factor which describes the toxicity of different pollutants in relation to their reactivity and site selectivity [48]. The biological activity of drug receptor interaction is illustrated from the value of electrophilicity. The new reactivity index is utilized to measure the stabilization energy when additional electronic charge from the environment from the system is needed. The measurements of the molecular stability and reactivity depend on the values of η and σ. The metal ion acts as a Lewis acid while **APA** behaves as a Lewis base in chelate formation.

3.5.3. Molecular Electrostatic Potential (MEP)

The electrostatic potential mapped onto the constant electron density surface is obtained from the plot of MEP. Also, it is important in disquisition of the molecular structure with its physiochemical property nexus and hydrogen bonding interplay [49] [50] [51]. The values of $V(r)$ at r (x, y, and z) is mooted in terms of the interaction energy between the electrical charge formed from the electrons of molecule, nuclei and proton located at r [52] [53]. The plot of 3D of MEP for **APA** is labeled in **Figure 10**. The results showed that the maximum negative

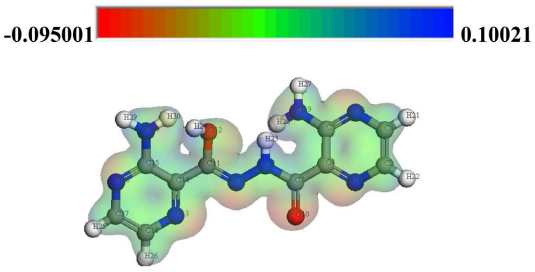

Figure 10. Molecular electrostatic potential of APA.

region suggests the most suitable site for electrophilic attack which symbolized by a red color. The blue color represents the maximum positive region prefers site for nucleophile attack. Equivocally the increase of potential is in the order red < green < blue, where blue depicts the strongest attraction and red shows the strongest repulsion. The negative potential regions are existed over the more electronegative atoms meanwhile the regions with positive potential are found over the hydrogen atoms.

3.5.4. Other Molecular Properties

Binding energy estimations detect that the increase of the value of calculated binding energy of complexes in comparison to that of **APA** indicating that the stability of the formed metal chelate is higher than that of **APA**. DFT calculations conjecture this energy as shown in Table 4.

3.6. Thermal Studies (TGA/DTG)

The degradable stages, temperature ranges degradable products as well as the weight loss percentages of Cu^{2+} chelate are shown in Table S11. Also, Figure S8 illustrates the TGA/DTG curves of the chelate. The results suggest that the experimental weight loss agrees with the calculated values. The residue was confirmed by chemical analysis. The first stage at 32˚C - 102˚C with weight loss of 3.3 (Calcd. 3.3%) matches to the loss of H_2O (lattice molecules) was shown from the TG thermogram of $C_{10}H_{13}Cu_2N_8O_4Cl_3$. The weight loss of 27.1 (Calcd. 27.2%) at 102˚C - 246˚C is assigned to the loss of the coordination water molecules and ($C_4H_4N_3$ + Cl) portions as shown from the second step. The removal of ($C_4H_3N_3$) portions with weight loss of 17.1 (Calcd. 17.2%) at 247˚C - 336˚C is obtained from the third step. The fourth step at 336˚C - 416˚C with weight wastage of 14.1 (Calcd. 13.4%) indicates the removal of 2HCl molecules. Finally, the fifth step is noticed in the 417˚C - 569˚C range with gradual mass loss corresponds to (N_2 + C) fragments, 7.3 (Calcd. 7.4%). The final remainder is $[Cu_2(O)_2]$ + C (Found 31.1, Calcd. 31.5%).

3.7. Biological Studies

3.7.1. The Antioxidant Activity

Antioxidant activity utilizing superoxide dismutase like activity assay was used

Table 4. Some of energetic properties of **APA** and its complexes calculated by DMOL^3 using DFT-method.

Compound	HOMO (eV)	LOMO (eV)	Binding energy (Kcal/mol)	Total energy (Kcal/mol)	Dipole moment (D)
APA	−5.027	−2.493	−3368.8	-6.1×10^5	6.9624
$C_{10}H_{13}Cu_2N_8O_4Cl_3$	−5.199	−3.265	−4185.1	-1.8×10^6	6.6597
$C_{12}H_{18}Co_2N_8O_5Cl_2$	−4.485	−3.632	−4043.2	-1.4×10^6	5.0550
$C_{14}H_{25}PtN_8O_6Cl_3$	−5.516	−4.034	−3756.7	-1.6×10^6	8.9002
$C_{11}H_{14}PdN_8O_{7/2}Cl$	−4.909	−3.462	−3619.9	-1.0×10^6	7.6981

to check out all the chelates. In contrarily, the Pd^{2+} chelate shows no antioxidant activity while **APA** showed from low to mediate anti-oxidative activity as shown in Figure 11.

The Cu^{2+}, Co^{2+} and Pt^{4+} chelates have the highest activity of quenching phenazin methosulphate radicals at 76.3%, 83.0% and 88.1% inhibition, respectively. The high potency of antioxidant is due to the fared of chelation. This is due to structure-activity relationship: they differ in the coordination geometries and stability and distortion. Moreover, the difference in the dipole moment of the complexes affects the stability, the distortion and the activity of the complexes. The compounds under investigation are considered as important group of promising antioxidants and also help to attenuate oxidative stress and used in protection against the harmful action of reactive oxygen species, mainly oxygen free radicals.

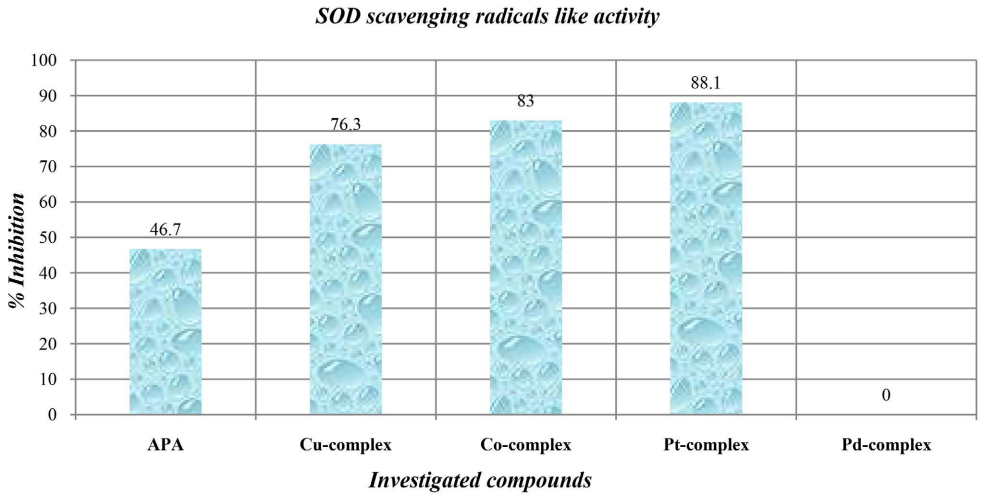

Figure 11. Superoxide dismutase scavenging radicals like activity of **APA** and its chelates.

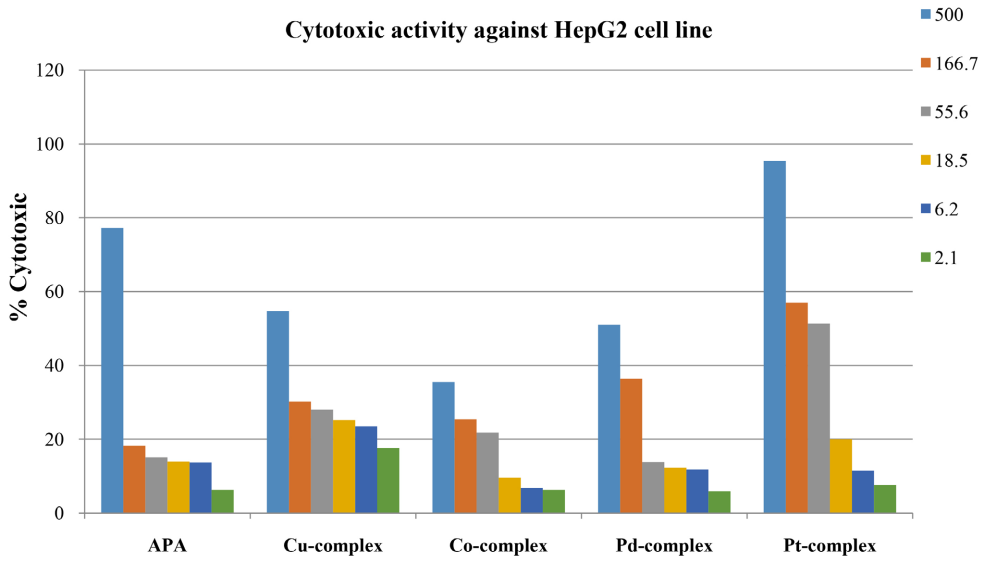

Figure 12. Cytotoxic activity of **APA** and its chelates.

3.7.2. Cytotoxic and Antitumor Activity

APA and its metal chelates were tried against hepatocellular carcinoma cell line HepG2 for their antitumor activity (Figure 12). After few days' incubation of the HepG2 liver cancer cells using different concentrations of **APA** and its chelates, Pt^{4+} proved to have the highest cytotoxic activity with IC_{50} of 79.8 μM.

The viability of HepG2 tumor cells after incubation with Pt^{4+} chelate is highly affected. The cell layer partially condensed forming cell-free areas and finally detached from the culture plate. **APA** and its chelates (Cu^{2+}, Co^{2+} and Pd^{2+}) show no significant cytotoxic activity. The data indicate that there is no significant difference in cell death in comparison to the untreated control (negative control).

4. Conclusion

Metal chelates (Cu^{2+}, Co^{2+}, Pt^{4+} and Pd^{2+}) derived from the novel ligand, (Z)-3-amino-N-(3-aminopyrazine-2-carbonyl) pyrazine-2-carbohydrazonic acid (**APA**, **L**) were synthesized and achieved by conventional physical and chemical, spectroscopic, magnetic and TGA studies. **APA** behaves in tridentate and tetradentate manners as in the case of Cu^{2+} and Co^{2+}, respectively. Also, the ligand acts in a bidentate manner towards Pt^{4+} and Pd^{2+} chelates. Both the corrected μ_{eff} and spectral data propose the geometries of the chelates and the molecular modeling. The chemical activity, energy components and also MEP for **APA** are figured out. *In Vitro*, cytotoxic activity and superoxide dismutase radical scavenger-like activity of the synthesized compounds HepG2 liver cancer cells were examined. Metal chelates show the potent anti-oxidative activity. The results of cytotoxic activity assay against hepatocellular carcinoma cell line HepG2 confirmed that Pt^{4+} complex has the highest value, while **APA**, Cu^{2+}, Co^{2+} and Pd^{2+} chelates have no significant cytotoxic activity.

Conflicts of Interest

The authors declare that they have no conflict of interests that could influence this work.

References

[1] Kerru, N., Gummidi, L., Maddila, S., Gangu, K.K. and Jonnalagadda, S.B. (2020) A Review on Recent Advances in Nitrogen-Containing Molecules and Their Biological Applications. *Molecules*, **25**, 1909-1951. https://doi.org/10.3390/molecules25081909

[2] Jampilek, J. (2019) Heterocycles in Medicinal Chemistry. *Molecules*, **24**, 3839-3842. https://doi.org/10.3390/molecules24213839

[3] Hosseinzadeh, Z., Ramazani, A. and Razzaghi-Asl, N. (2018) Anti-Cancer Nitrogen-Containing Heterocyclic Compounds. *Current Organic Chemistry*, **23**, 2256-2279. https://doi.org/10.2174/1385272822666181008142138

[4] Shetty, N and Gupta, S. (2014) Eribulin Drug Review. *South Asian Journal of Cancer*, **3**, 57-59. https://doi.org/10.4103/2278-330X.126527

[5] Welsh, S and Corrie, P (2015) Management of BRAF and MEK Inhibitor Toxicities in Patients with Metastatic Melanoma. *Therapeutic Advances in Medical Oncology*,

7, 122-136. https://doi.org/10.1177/1758834014566428

[6] Kakkar, S., Kumar, S., Narasimhan1, B., Lim, S.M, Ramasamy, K. Mani, V. and Shah, S.A.A. (2018) Design, Synthesis and Biological Potential of Heterocyclic Benzoxazole Scaffolds as Promising Antimicrobial and Anticancer Agents. *Chemistry Central Journal*, **96**, Article No. 96. https://doi.org/10.1186/s13065-018-0464-8

[7] Schneider, M.R. (1987) Hydroxy Substituted 10-Ethyl-9-phenylphenanthrenes: Compounds for the Investigation of the Influence of E, Z-Isomerization on the Biological Properties of Tumor Inhibiting 1.1.2-Triphenylbutenes. *Archiv der Pharmazie*, **320**, 159-166. https://doi.org/10.1002/ardp.19873200212

[8] Nawrocka, W. and Stasko, J. (1997) New Derivatives of 3Amino-2(1H)-Thioxo-4(3H)-Quinazolinone. Part II. Reaction of 3-Amino-2(1H)-Thioxo-4(3H)-Quinazolinone with Cyanogen Bromide. *Polish Journal of Chemistry*, **71**, 792-796.

[9] Nawrocka, W., Sztuba, B., Drys, A., Wietrzyk, J., Kosendiak, J. and Opolski, A. (2014) Synthesis and AntiProliferative Activity *in vitro* of New 2-Aminobenzimidazole Derivatives. Reaction of 2-Arylideneaminobenzimidazole with Selected Nitriles Containing Active Methylene Group. *Central European Journal of Chem*istry, **12**, 1047-1055. https://doi.org/10.2478/s11532-014-0533-3

[10] Milczarska, B., Gobis, K., Foks, H., Golunski, L.L. and Sowinski, P. (2012) The Synthesis of 3-Amino-Pyrazine-2-Carbohydrazide and 3-Amino-N'-Methylpyrazine-2-Carbohydrazide Derivatives. *Heterocyclic Chem*istry, **49**, 845-850. https://doi.org/10.1002/jhet.877

[11] Bergman, J. and Brynolf, A. (1990) Synthesis of Chrysogine, a Metabolite of *Penicillium chrysogenum* and Some Related 2-Substituted 4-(3H)-Quinazolinones. *Tetrahedron*, **46**, 1295-1310. https://doi.org/10.1016/S0040-4020(01)86694-1

[12] Jakobsen, P., Horneman, A.M. and Persson, E. (2000) Inhibitors of the Tissue Factor/Factor VIIa-Induced Coagulation: Synthesis and *in Vitro* Evaluation of Novel 2-Aryl Substituted Pyrid. *Bioorganic & Medicinal Chemistry*, **8**, 2803-2812.

[13] Maga, J.A. (1992) Pyrazine Update. *Food Reviews International*, **8**, 479-558. https://doi.org/10.1080/87559129209540951

[14] Yamaguchi, T., Ito, S., Kashige, N., Nakahara, K. and Harano, K. (2007) The Relationship between the Chemical Structures of Dihydropyrazine Derivatives and DNA Strand-Breakage Activity. *Chemical and Pharmaceutical Bulletin*, **55**, 532-536. https://doi.org/10.1248/cpb.55.532

[15] Dolezal, M. (2006) Biologically Active Pyrazines of Natural and Synthetic Origin. *Chemické Listy*, **100**, 959-966.

[16] Vogel, A.I. (1961) A Text Book of Quantitative Inorganic Analysis. Longmans, London.

[17] Bain, G.A. and John, F. (2008) Diamagnetic Corrections and Pascal's Constant. *Journal of Chemical Education*, **85**, 532-536. https://doi.org/10.1021/ed085p532

[18] Nishikimi, M., Appaji, N. and Yagi, K. (1972) The Occurrence of Superoxide Anion in the Reaction of Reduced Phenazine Methosulfate and Molecular Oxygen. *Biochemical and Biophysical Research Communications*, **46**, 849-854. https://doi.org/10.1016/S0006-291X(72)80218-3

[19] Selvakumaran, M., (2003) Enhanced Cisplatin Cytotoxicity by Disturbing the Nucleotide Excision Repair Pathway in Ovarian Cancer Cell Line. *Cancer Research*, **63**, 1311-3116.

[20] Delley, B. (1990) An All-Electron Numerical Method for Solving the Local Density Functional or Pyatomic Molecules. *Journal of Chemical Physics*, **92**, 508-517. https://doi.org/10.1063/1.458452

[21] Materials Studio 6.0 Copyright (2009) Accelrys Software Inc.

[22] Hehre, W.J., Radom, L., Schleyer, P.V.R. and Pople, J.A. (1986) *Ab Initio* Molecular Orbital Theory. John Wiley & Sons, New York.

[23] Hammer, B., Hansen, L.B. and Nørskov, J.K. (1999) Improved Adsorption Energetics within Density-Functional Theory Using Revised Perdew-Burke-Ernzerh of functionals. *Physical Review B*, **59**, 7413-7421. https://doi.org/10.1103/PhysRevB.59.7413

[24] Matveev, A., Staufer, M., Mayer, M. and Roesch, N. (1999) Density Functional Study of Small Molecules and Transition-Metal Carbonyls Using Revised PBE Functional. *International Journal of Quantum Chemistry*, **75**, 863-873. https://doi.org/10.1002/(SICI)1097-461X(1999)75:4/5<863::AID-QUA51>3.0.CO;2-T

[25] Geary, W.J. (1971) The Use of Conductivity Measurements in Organic Solvents for the Characterization of Coordination Compounds. *Coordination Chemistry Reviews*, **7**, 81-122. https://doi.org/10.1016/S0010-8545(00)80009-0

[26] Ketcham, K.A., Garcia, I., Swearingen, J.K., El-Sawaf, A.K., Bermejo, E., Castineiras, A. and West, D.X. (2002) Spectral Studies and X-Ray Crystal Structures of Three Nickel(II) Complexes of 2-Pyridineformamide 3-Piperidylthiosemicarbazon. *Polyhedron*, **21**, 859-865. https://doi.org/10.1016/S0277-5387(02)00853-7

[27] Salah, S., El-Wahab, A., Zeinab, H., Farag, R.S. and Mostafa, M.M. (2014) Synthesis, Characterization and Modeling Structures of Isatin-3-Girard T (IGT) and P (IGP) Hydrazone Complexes. *Spectrochimica Acta*, **124**, 579-587. https://doi.org/10.1016/j.saa.2014.01.082

[28] Alpert, N.L., Keiser, W.E. and Szmanski, H.A. (1970) IR Theory and Practice of Infrared Spectroscopy, Plenum Press, New York. https://doi.org/10.1007/978-1-4684-8160-0_1

[29] Azhari, S.J., Mlahi, M.R., Al-Asmy, A.A. and Mostafa, M.M. (2015) Synthesis of Novel Binary and Ternary Complexes Derived from 1-(2-Hydroxybenzoyl)-4-Phenylthiosemicarbazide (L^1) and 2,2'-Dipyridyl (L^2) with Co^{II}, Cu^{II} and Zn^{II} Salts. *Spectrochimica Acta*, **36**, 185-191. https://doi.org/10.1016/j.saa.2014.09.012

[30] Nakamoto, K. (2009) Infrared and Raman Spectra of Inorganic and Coordination Compounds. 6th Edition, John Wiley and Sons, Inc., Hoboken. https://doi.org/10.1002/9780470405840

[31] Ferraro, J.R. and Walker, W.R. (1965) Infrared Spectra of Hydroxy-Bridged Copper(II) Compounds. *Inorganic Chemistry*, **4**, 1382-1386. https://doi.org/10.1021/ic50032a002

[32] Rageovic, K.C., Kakurinov, V.V., Molnar, D.G. and Buzarovska, A. (2001) Synthesis, Antibacterial and Antifungal Activity of 4-Substituted-5-Aryl-1,2,4-Triazoles. *Molecules*, **6**, 815-824. https://doi.org/10.3390/61000815

[33] Ramachandran, R., Rani, M. and Kabilan, S.J. (2010) Synthesis, Structure and Conformational Analysis of 2,4-diaryl-3-azabicyclo[3.3.1]nonan-9-one Thiosemicarbazones and Semicarbazones. *Journal of Molecular Structure*, **970**, 42-50. https://doi.org/10.1016/j.molstruc.2010.02.005

[34] Kidrič, J., Hadži, D., Kocjan, D. and Rutar, V. (1981) ^{1}H and ^{13}C NMR Study of 8-Hydroxyquinoline and Some of Its 5-Substituted Analogues. *Organic Magnetic Resonance*, **15**, 280-284. https://doi.org/10.1002/mrc.1270150314

[35] Silverstein R.M. and Bassler, G.C. (1967) Spectroscopic Identification of Organic Compounds. Wiley, New York.

[36] Tossidis, I.A., Bolos, C.A., Aslinidis, P.N. and Katsoulos, G.A. (1987) Monohaloge-

nobenzoylhydrazones III. Synthesis and Structural Studies of Pt(II), Pd(II) and Rh(III) Complexes of Di-(Pyridyl)Ketonechlorobenzoyl Hydrazones. *Inorganica Chimica Acta,* **133**, 275-280. https://doi.org/10.1016/S0020-1693(00)87779-8

[37] Rao, C.N.R. (1975) Ultraviolet and Visible Spectroscopy. Plenum Press, New York.

[38] Lever, A.B.P. (1968) Inorganic Electronic Spectroscopy. Elsevier, Amsterdam.

[39] Kato, M., Jonassen, K.B. and Fanning, G.C. (1964) Copper(II) Complexes with Subnormal Magnetic Moments. *Chemical Reviews*, **64**, 99-128. https://doi.org/10.1021/cr60228a003

[40] Kettle, S.F.A. (1969) Coordination Compounds. Thomas Nelson and Sons Let, London.

[41] Lewis, J. and Wilkins, R.G. (1960) Modern Coordination Chemistry. Interscince, New York.

[42] Al-assy, W.H., El-askalany, A.H. and Mostafa, M.M. (2013) Structural Comparative Studies on New Mn(II), Cr(III) and Ru(III) Complexes Derived from 2,4,6-Tri-(2-Pyridyl)-1,3,5-Triazine (TPTZ) *Spectrochimica Acta*, **116**, 401-407. https://doi.org/10.1016/j.saa.2013.07.086

[43] Yousef, T.A., El-Reash, G.M.A. and El Morshedy, R.M. (2012) Quantum Chemical Calculations, Experimental Investigations and DNA Studies on (E)2-((3-Hydroxy-Naphthalen-2-yl) Methylene)-N-(Pyridin-2-yl) Hydrazine Carbothioamide and Its Mn(II), Ni(II), Cu(II), Zn(II) and Cd(II) Complexes. *Polyhedron,* **45**, 71-85. https://doi.org/10.1016/j.poly.2012.07.041

[44] Linert, W. and Taha, A. (1994) Co-ordination of Solvent Molecules to Square-Planar Mixed-Ligand Nickel(II) Complexes. A Thermodynamic and Quantum-Mechanical Study. *Journal of the Chemical Society*, *Dalton Transactions*, **7**, 1091-1095. https://doi.org/10.1039/dt9940001091

[45] Govindarajan, M., Periandy, S. and Carthigayen, K. (2012) FT-IR and FT-Raman Spectra, Thermodynamical Behavior, HOMO and LUMO, UV, NLO Properties, Computed Frequency Estimation Analysis and Electronic Structure Calculations on α-Bromotoluene. *Spectrochimica Acta*, **97**, 41-422. https://doi.org/10.1016/j.saa.2012.06.028

[46] Pearson, R.G. (1989) Estimating Vorization Enthalpies of Organic Compounds with Single and Multiple Substitution. *The Journal of Organic Chemistry*, **54**, 5250-5256. https://doi.org/10.1021/jo00283a016

[47] Padmanabhan, J., Parthasarathi, R., Subramanian, V. and Chattaraj, P. (2007) Density Functional Tanalysis of Molybdenum Isotope Fractionation. *The Journal of Physical Chemistry A*, **111**, 12434-12438. https://doi.org/10.1021/jp074318q

[48] Parthasarathi, R., Padmanabhan, J., Sarkar, U., Maiti, B., Subramanian, V. and Chattaraj, P.K. (2003) Toxicity Analysis of Benzidine through Chemical Reactivity and Selectivity Profiles: A DFT Approach. *Internet Electronic Journal of Molecular Design*, **2**, 798-813.

[49] Scrocco, E. and Tomasi, J. (1978) Electronic Molecular Structure, Advances in Quantum Chemistry. Academic Press, Cambridge, MA.

[50] Luque, F.J., López, J.M. and Orozco, M. (2000) Perspective on "Electrostatic Interactions of a Solute with a Continuum. A Direct Utilization of *Ab initio* Molecular Potentials for the Prevision of Solvent Effects". *Theoretical Chemistry Accounts*, **103**, 343-345. https://doi.org/10.1007/s002149900013

[51] Okulik, N. and Ubert, A.H.J. (2005) Theoretical Analysis of the Reactivity Sites of Non-Inflammatory Drugs. *Internet Electronic Journal of Molecular Design*, **4**,

17-30.

[52] Politzer, P., Laurence, P.R. and Jayasuriya, K. (1985) Molecular Electrostatic Potentials: An Effective Tool for the Elucidation of Biochemical Phenomena. *Environmental Health Perspectives*, **61**, 191-202. https://doi.org/10.1289/ehp.8561191

[53] Scrocco, E. and Tomasi, J. (1973) The Electrostatic Molecular Potential as a Tool for the Interpretation of Molecular Properties. In: *New Concepts II*, *Topics in Current Chemistry Fortschritte der Chemischen Forschung*, Vol. 42, Springer, Berlin, 95-170.

Appendix

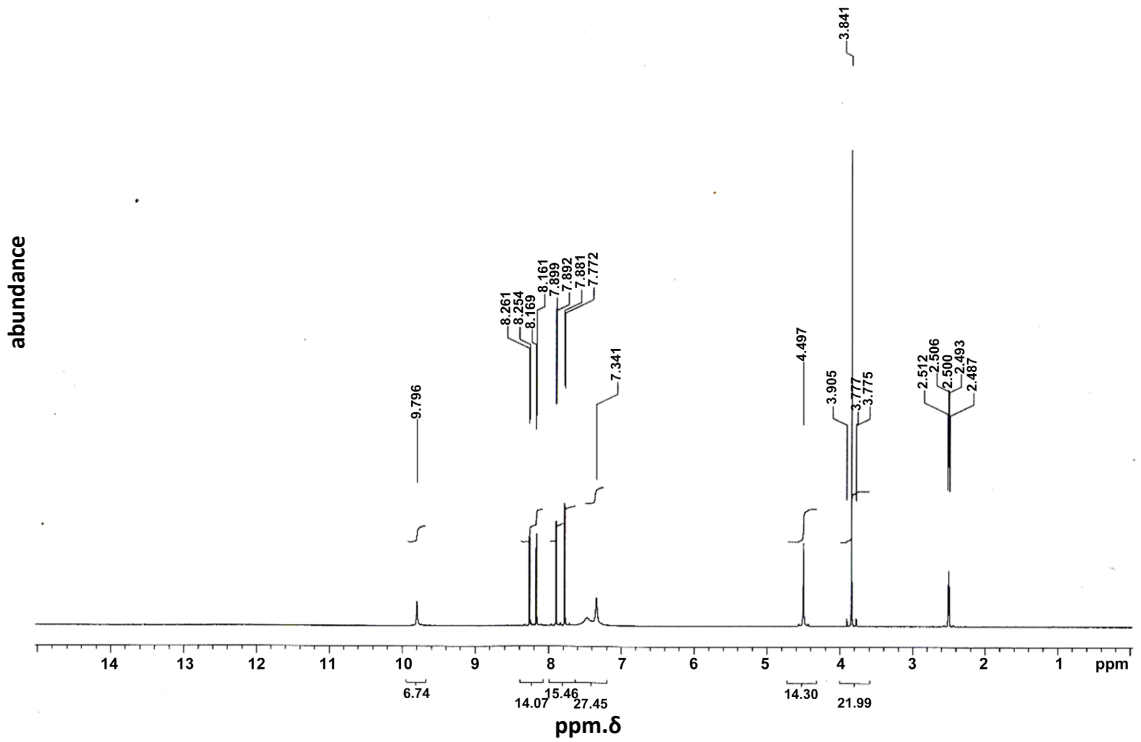

Figure S1. ^{1}H-NMR spectrum of **APA** in d_6-DMSO.

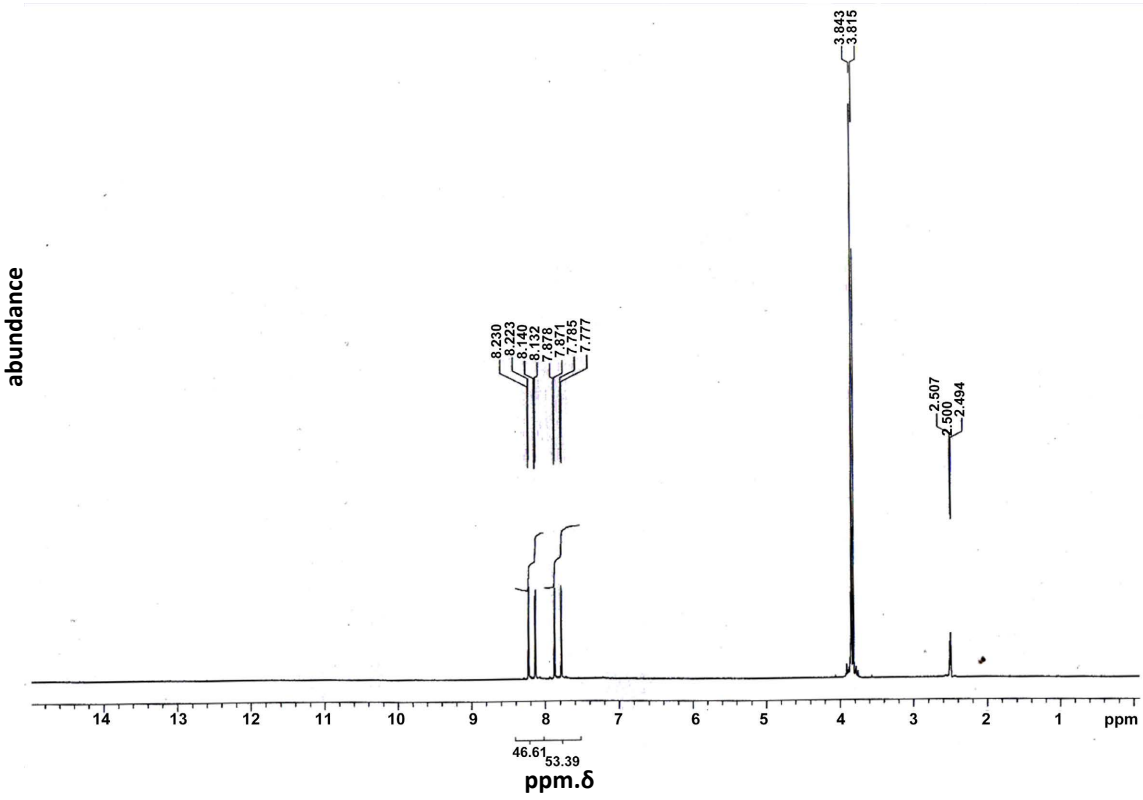

Figure S2. ^{1}H-NMR spectrum of **APA** in d_6-DMSO and D_2O.

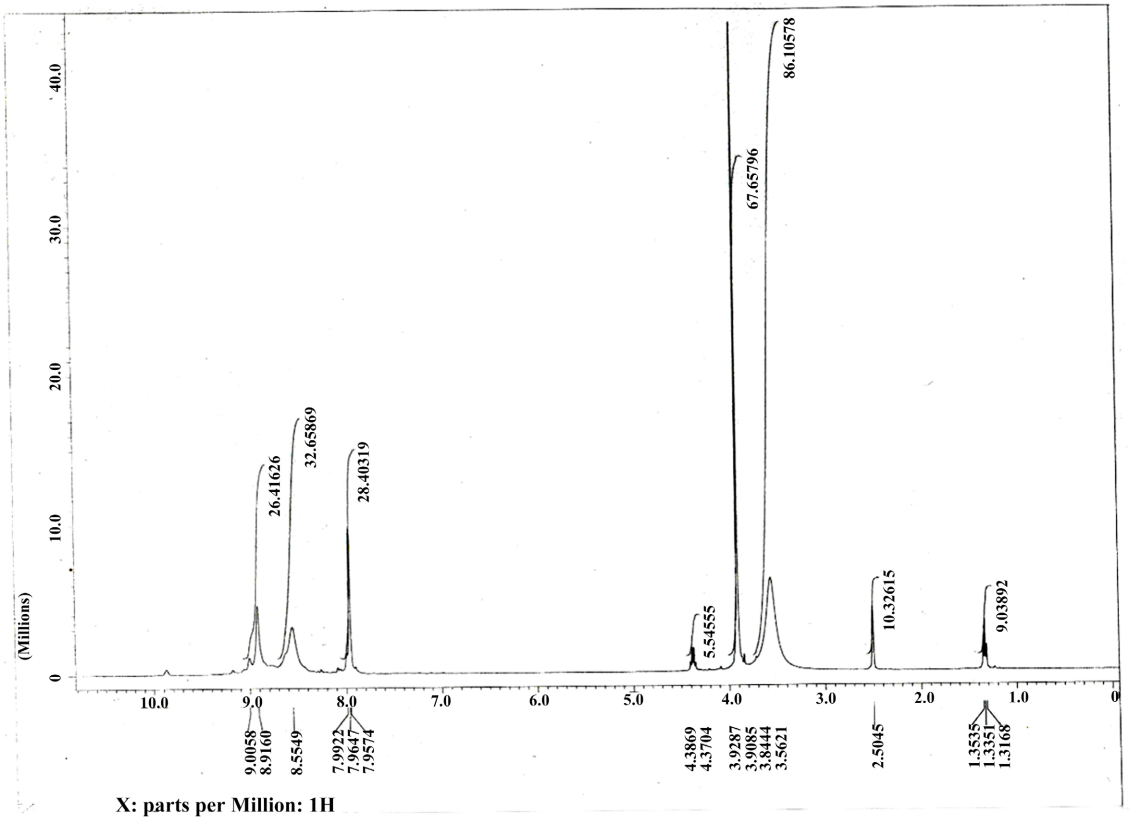

Figure S3. ^{1}H-NMR spectrum of [Pt(**APA**-H)(H_2O)Cl_3]·H_2O·2EtOH in d_6-DMSO.

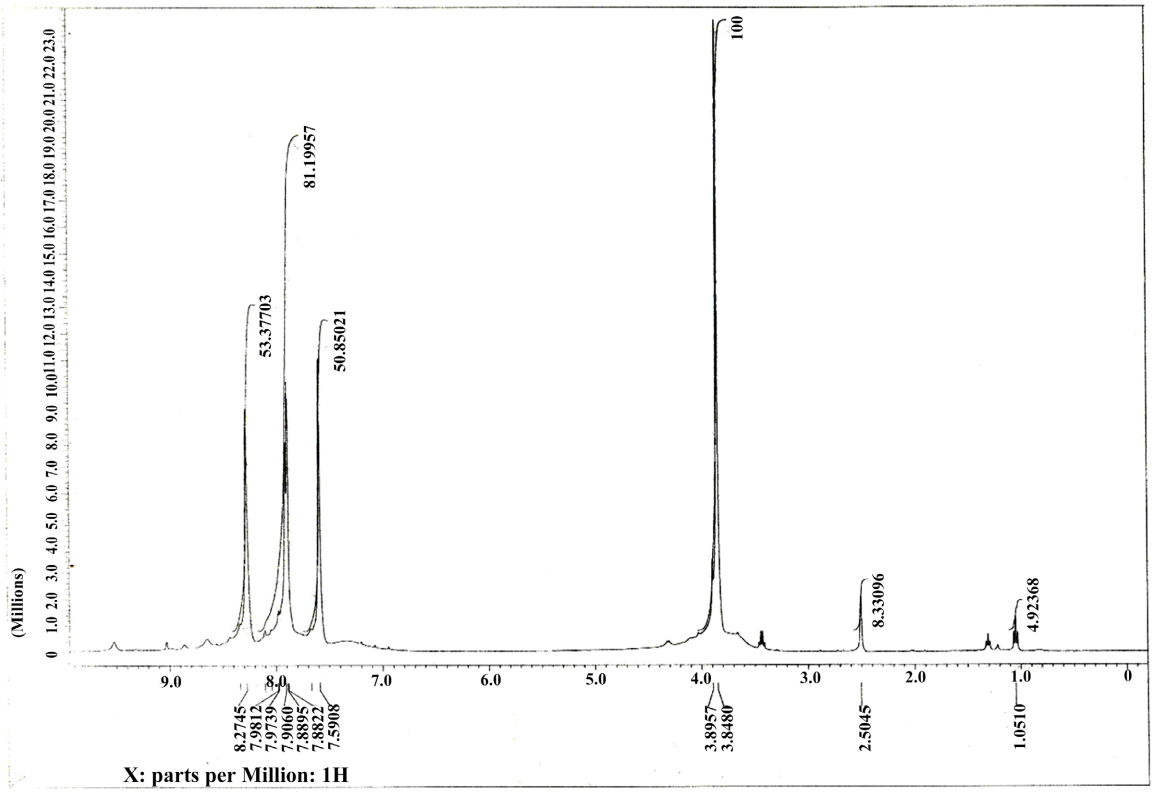

Figure S4. ^{1}H-NMR spectrum of [Pd(**APA**-H)(H_2O)Cl]·1/2EtOH in d_6 DMSO.

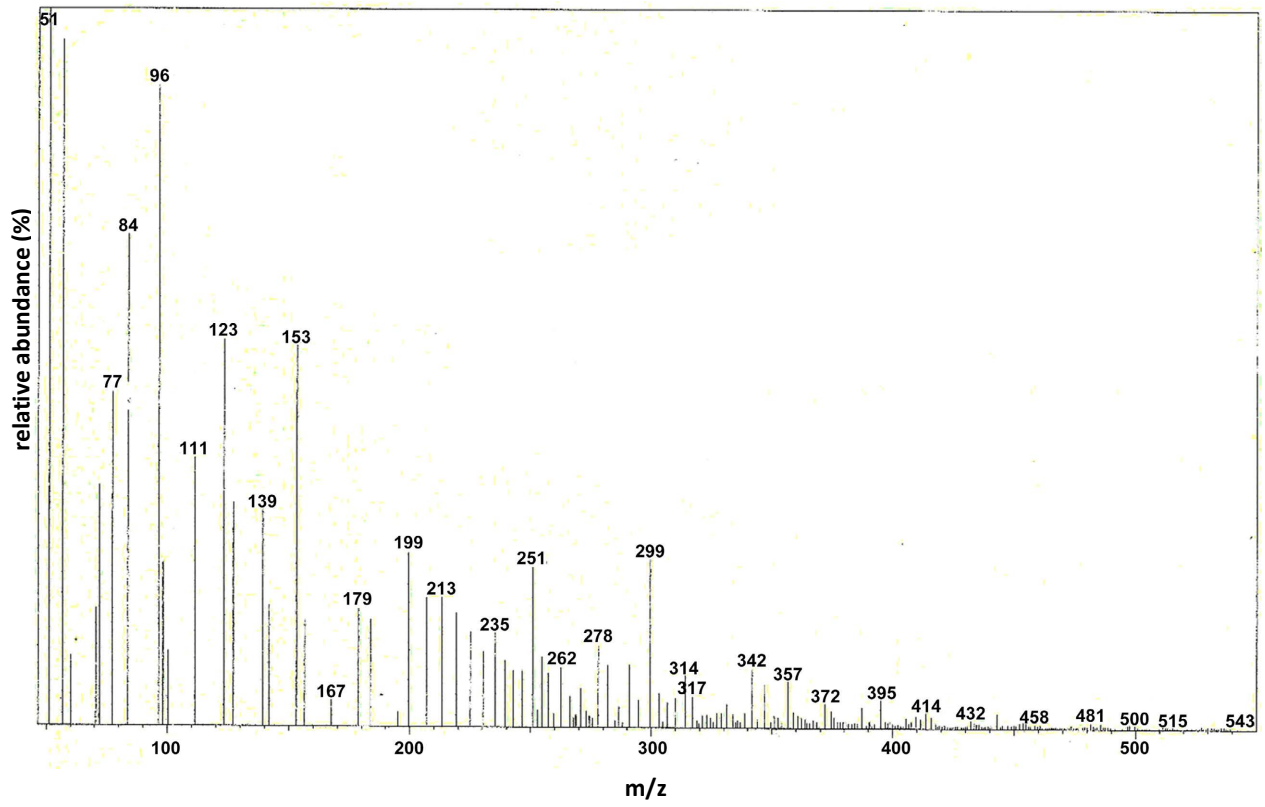

Figure S5. Mass spectrum of $[Co_2(\mathbf{APA}\text{-}2H)(H_2O)_2Cl_2]\cdot EtOH$.

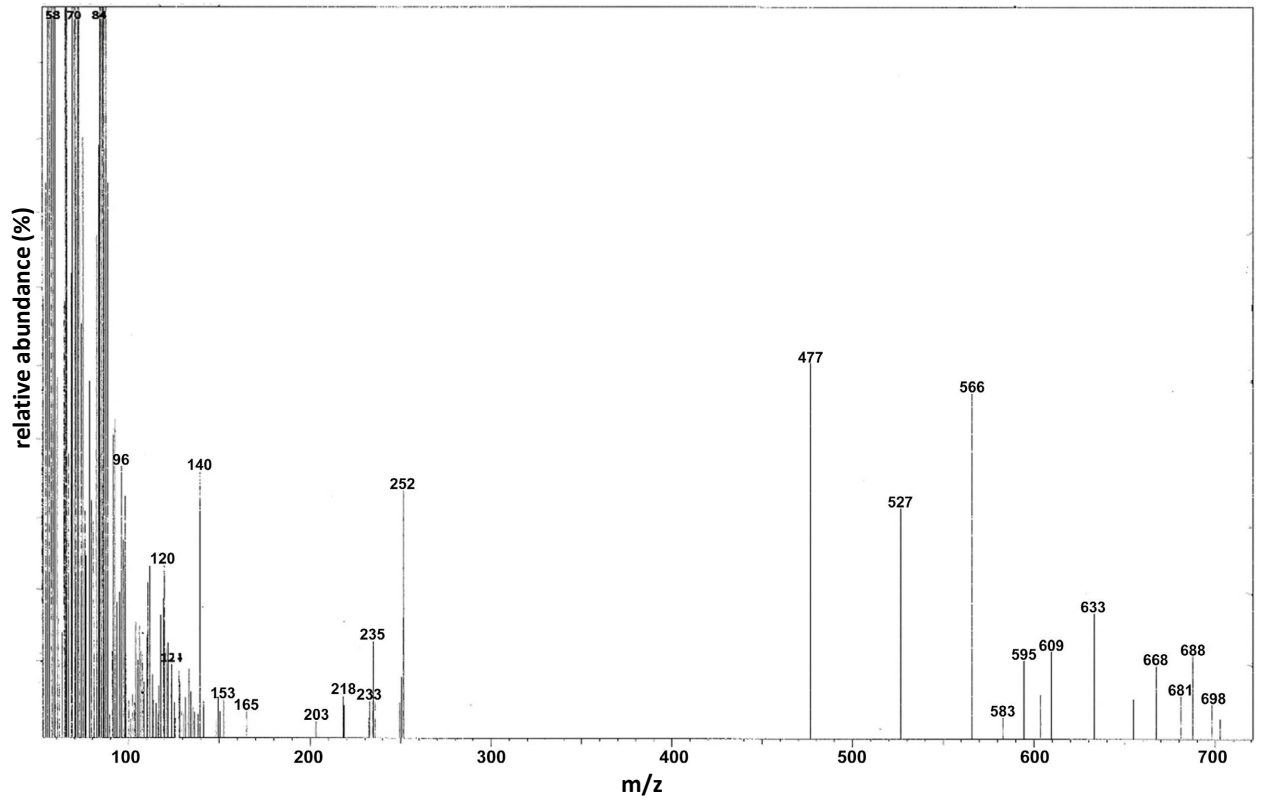

Figure S6. Mass spectrum of $[Pt(\mathbf{APA}\text{-}H)(H_2O)Cl_3]\cdot H_2O\cdot 2EtOH$.

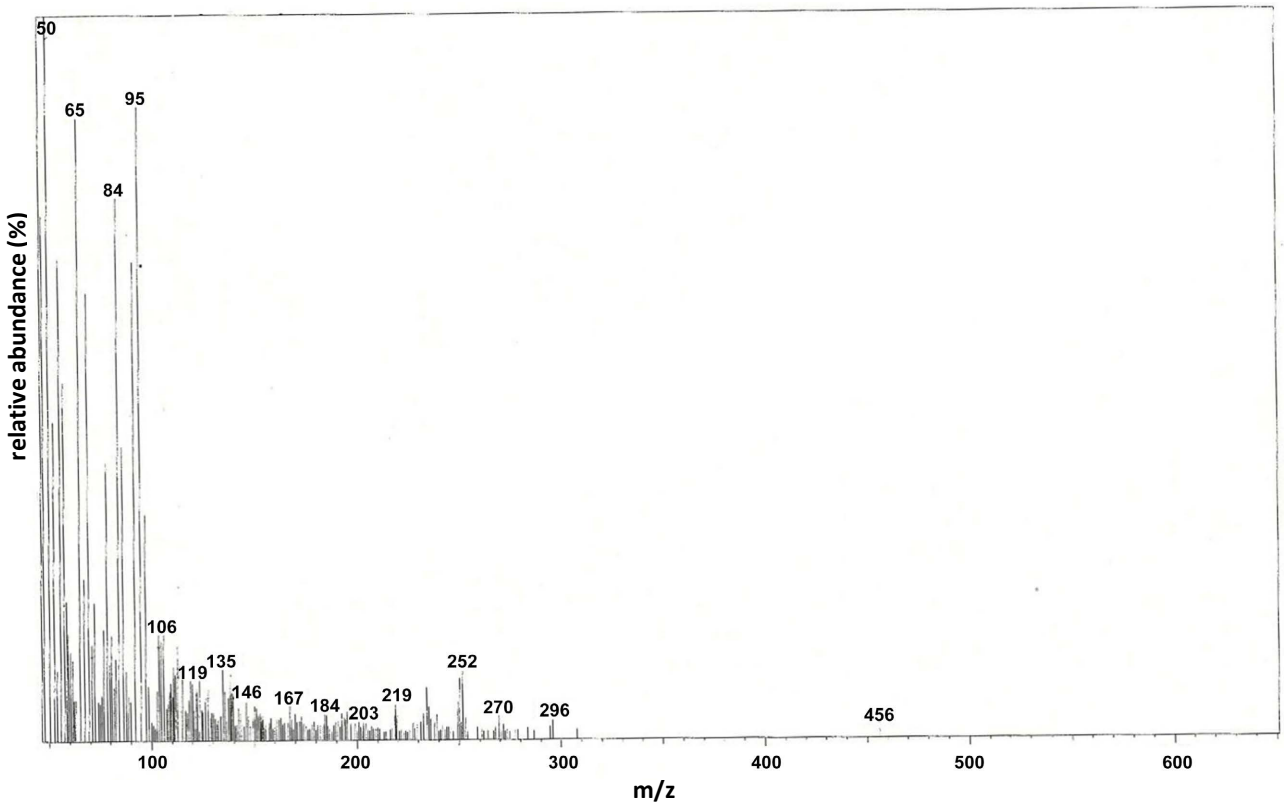

Figure S7. Mass spectrum of [Pd(**APA**-H)(H_2O)Cl]·1/2EtOH.

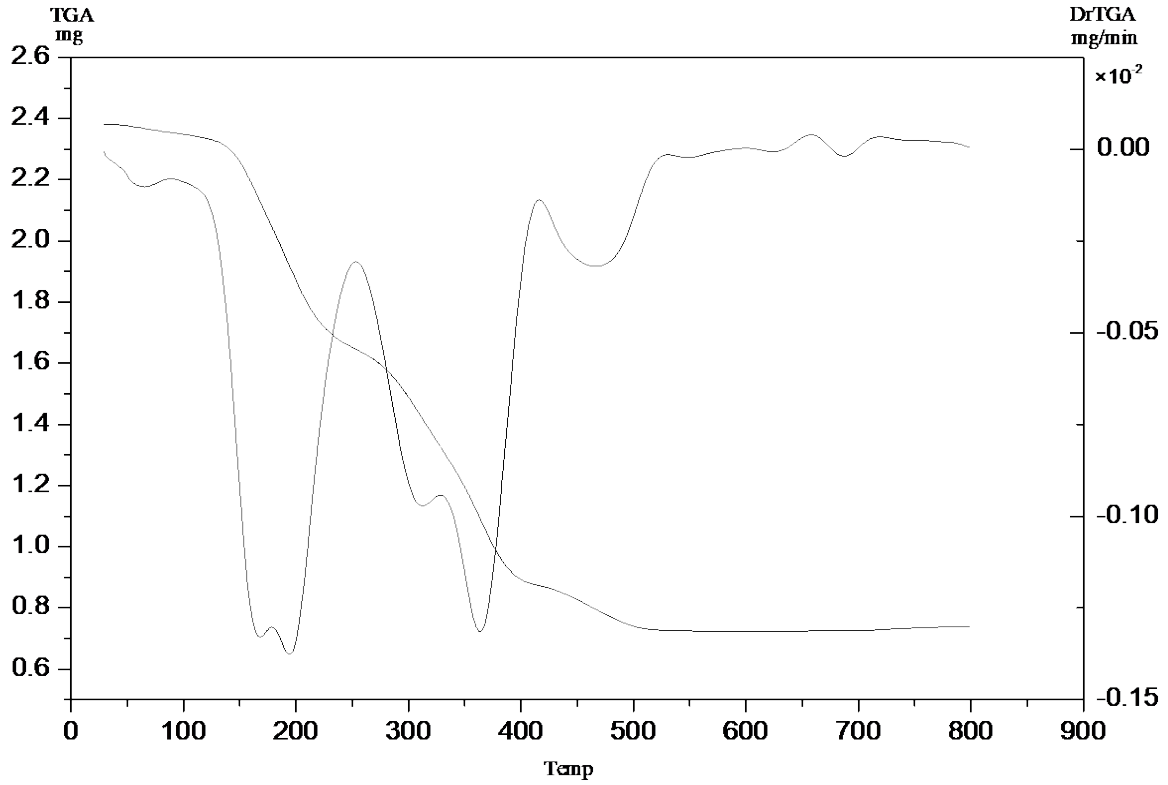

Figure S8. Thermal analysis curves (TGA, DTG) of [Cu_2(**APA**-H)(H_2O)Cl_3]·H_2O.

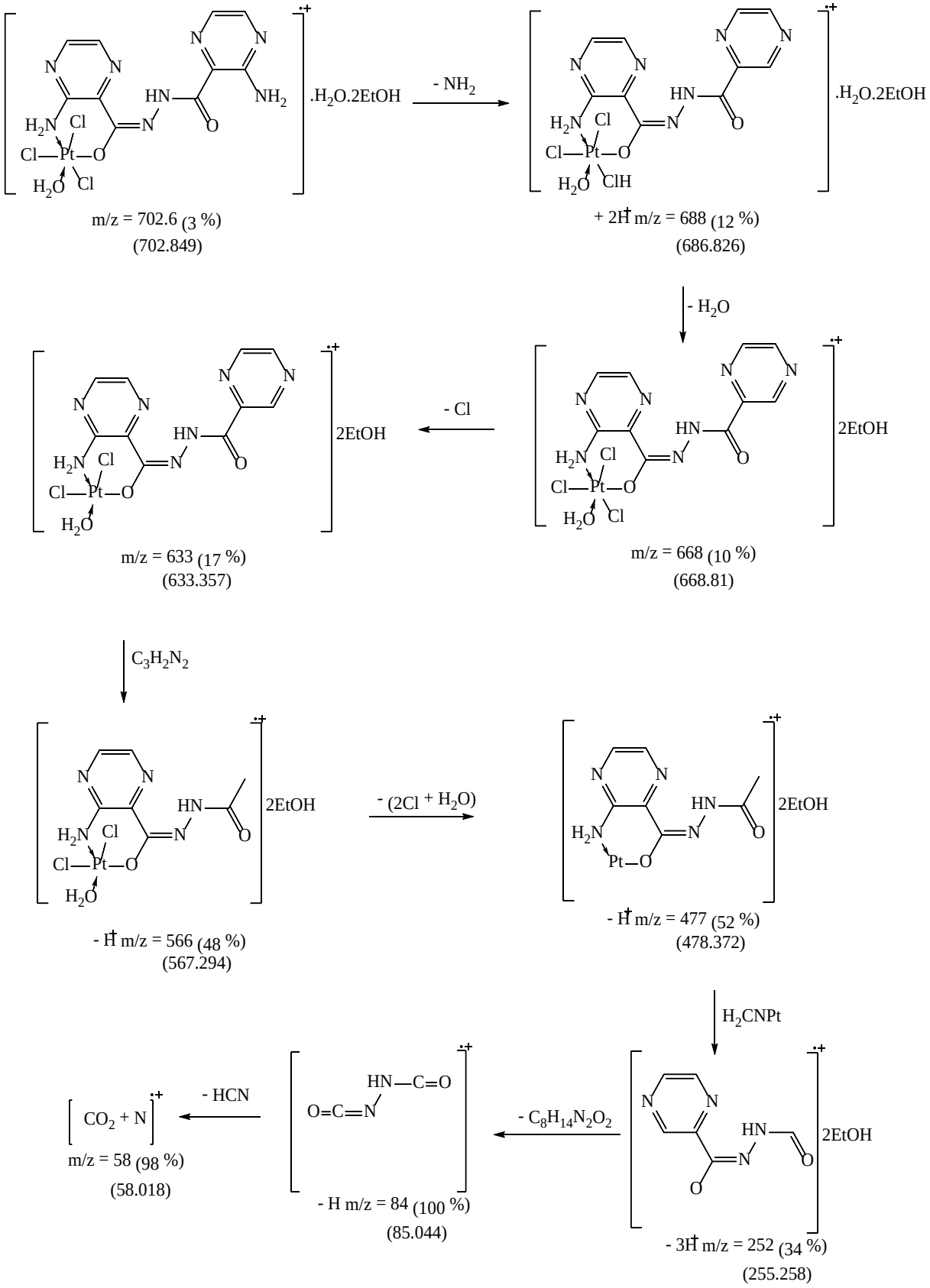

Scheme S1. The main fragments in mass spectrum of [Pt(**APA**)-H(H_2O)Cl_3]·H_2O·2EtOH.

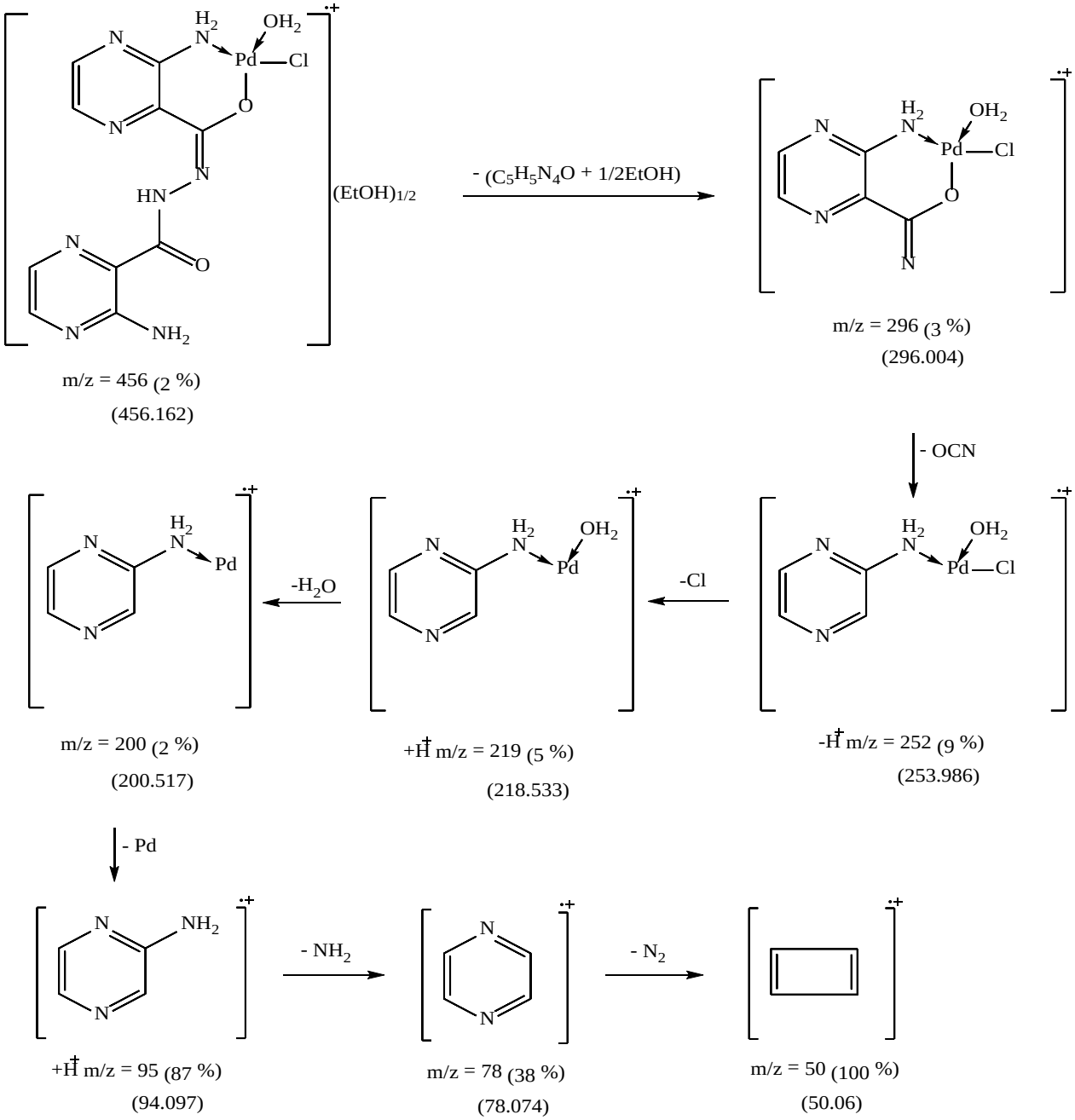

Scheme S2. The main fragments in mass spectrum of [Pd(**APA**-H)(H_2O)Cl]·1/2EtOH.

Table S1. Bonds lengths (Å) of (**APA**) using DFT-method from DMOL^3 calculations.

Bond	Length (Å)	Bond	Length (Å)	Bond	Length (Å)	Bond	Length (Å)
N(20)-H(30)	1.1078	C(15)-N(20)	1.5109	N(9)-C(11)	1.5095	C(4)-C(5)	1.5426
N(20)-H(29)	1.1098	C(15)-N(16)	1.5098	N(8)-H(23)	1.1087	N(3)-C(4)	1.5095
N(19)-H(28)	1.1089	C(14)-C(15)	1.5438	N(8)-N(9)	1.479	C(2)-H(22)	1.1399
N(19)-H(27)	1.1099	C(18)-N(13)	1.5095	C(7)-O(10)	1.5103	C(2)-N(3)	1.5102
C(18)-H(26)	1.14	N(13)-C(14)	1.5098	C(7)-N(8)	1.5099	C(1)-H(21)	1.1399
C(17)-H(25)	1.1398	O(12)-H(24)	1.11	C(5)-N(19)	1.5107	N(6)-C(1)	1.5094
C(17)-C(18)	1.5383	C(14)-C(11)	1.5419	C(5)-N(6)	1.5095	C(1)-C(2)	1.539
N(16)-C(17)	1.5088	C(11)-O(12)	1.5079	C(4)-C(7)	1.542		

Table S2. Bonds angles (˚) of (**APA**) using DFT-method from DMOL^3 calculations.

Angle	Degree (˚)	Angle	Degree (˚)	Angle	Degree (˚)
H(30)-N(20)-H(29)	119.8083	N(16)-C(15)-C(14)	119.8481	N(8)-C(7)-C(4)	120.0328
H(30)-N(20)-C(15)	120.4091	C(15)-C(14)-N(13)	119.7604	C(5)-N(6)-C(1)	120.1135
H(29)-N(20)-C(15)	119.7821	C(15)-C(14)-C(11)	120.849	N(19)-C(5)-N(6)	119.4975
H(28)-N(19)-H(27)	119.8783	N(13)-C(14)-C(11)	119.3906	N(19)-C(5)-C(4)	120.6217
H(28)-N(19)-C(5)	120.2226	C(18)-N(13)-C(14)	120.2529	N(6)-C(5)-C(4)	119.8576
H(27)-N(19)-C(5)	119.8853	H(24)-O(12)-C(11)	109.5015	C(7)-C(4)-C(5)	120.6503
H(26)-C(18)-C(17)	120.0106	C(14)-C(11)-O(12)	120.5572	C(7)-C(4)-N(3)	119.6208
H(26)-C(18)-N(13)	120.0344	C(14)-C(11)-N(9)	120.2337	C(5)-C(4)-N(3)	119.7171
C(17)-C(18)-N(13)	119.955	O(12)-C(11)-N(9)	119.1791	C(4)-N(3)-C(2)	120.108
H(25)-C(17)-C(18)	120.0382	C(11)-N(9)-N(8)	118.9125	H(22)-C(2)-N(3)	120.0437
H(25)-C(17)-N(16)	120.0359	H(23)-N(8)-N(9)	119.5355	H(22)-C(2)-C(1)	120.0059
C(18)-C(17)-N(16)	119.9258	H(23)-N(8)-C(7)	119.8885	N(3)-C(2)-C(1)	119.9495
C(17)-N(16)-C(15)	120.2461	N(9)-N(8)-C(7)	120.5228	H(21)-C(1)-N(6)	120.041
N(20)-C(15)-N(16)	119.2623	O(10)-C(7)-N(8)	119.9566	H(21)-C(1)-C(2)	120.0285
N(20)-C(15)-C(14)	120.8896	O(10)-C(7)-C(4)	119.9196	N(6)-C(1)-C(2)	119.9277

Table S3. Bonds lengths (Å) of $[Cu_2$(**APA**-H)$(H_2O)Cl_3]\cdot H_2O$ using DFT-method from DMOL calculations.

Bond	Length (Å)	Bond	Length (Å)	Bond	Length (Å)	Bond	Length (Å)
O(24)-H(37)	0.9973	N(19)-H(32)	1.0338	N(13)-C(14)	1.3817	C(5)-N(19)	1.4295
O(24)-H(36)	0.9973	N(19)-Cu(21)	2.2537	O(12)-Cu(22)	2.1144	C(5)-N(6)	1.3596
O(24)-Cu(22)	2.307	C(18)-H(31)	1.0959	C(14)-C(11)	1.4721	C(4)-C(7)	1.4618
Cl(23)-Cu(22)	2.3418	C(17)-H(30)	1.0955	C(11)-O(12)	1.3259	C(4)-C(5)	1.4461
Cl(26)-Cu(21)	2.35	C(17)-C(18)	1.4239	O(10)-Cu(21)	2.1479	N(3)-C(4)	1.383
Cl(25)-Cu(21)	2.3589	N(16)-C(17)	1.3642	N(9)-C(11)	1.3743	C(2)-H(28)	1.097
N(20)-H(35)	1.0358	C(15)-N(20)	1.4392	N(8)-H(29)	1.0488	C(2)-N(3)	1.3584
N(20)-H(34)	1.0389	C(15)-N(16)	1.3612	N(8)-N(9)	1.35	C(1)-H(27)	1.0968
N(20)-Cu(22)	2.2372	C(14)-C(15)	1.4531	C(7)-O(10)	1.3055	N(6)-C(1)	1.3614
N(19)-H(33)	1.0382	C(18)-N(13)	1.359	C(7)-N(8)	1.4	C(1)-C(2)	1.4276

Table S4. Bonds angles (˚) of $[Cu_2(\mathbf{APA}\text{-}H)(H_2O)Cl_3]\cdot H_2O$ using DFT-method from DMOL^3 calculations.

Angle	Degree (˚)	Angle	Degree (˚)	Angle	Degree (˚)
H(37)-O(24)-H(36)	104.086	H(33)-N(19)-C(5)	113.632	C(11)-N(9)-N(8)	119.668
H(37)-O(24)-Cu(22)	104.421	H(32)-N(19)-Cu(21)	111.1704	H(29)-N(8)-N(9)	118.3853
H(36)-O(24)-Cu(22)	109.2731	H(32)-N(19)-C(5)	109.4936	H(29)-N(8)-C(7)	119.973
O(24)-Cu(22)-Cl(23)	106.4758	Cu(21)-N(19)-C(5)	114.9949	N(9)-N(8)-C(7)	121.6032
O(24)-Cu(22)-N(20)	105.1124	H(31)-C(18)-C(17)	121.7454	O(10)-C(7)-N(8)	119.7595
O(24)-Cu(22)-O(12)	111.9968	H(31)-C(18)-N(13)	117.0667	O(10)-C(7)-C(4)	125.3761
Cl(23)-Cu(22)-N(20)	121.7634	C(17)-C(18)-N(13)	121.1866	N(8)-C(7)-C(4)	114.8569
Cl(23)-Cu(22)-O(12)	128.4852	H(30)-C(17)-C(18)	122.0378	C(5)-N(6)-C(1)	118.0727
N(20)-Cu(22)-O(12)	79.4743	H(30)-C(17)-N(16)	117.5059	N(19)-C(5)-N(6)	116.2464
Cl(26)-Cu(21)-Cl(25)	121.4286	C(18)-C(17)-N(16)	120.4563	N(19)-C(5)-C(4)	121.8344
Cl(26)-Cu(21)-N(19)	111.214	C(17)-N(16)-C(15)	118.5789	N(6)-C(5)-C(4)	121.8834
Cl(26)-Cu(21)-O(10)	116.756	N(20)-C(15)-N(16)	114.9991	C(7)-C(4)-C(5)	123.8421
Cl(25)-Cu(21)-N(19)	102.41	N(20)-C(15)-C(14)	123.0853	C(7)-C(4)-N(3)	117.6196
Cl(25)-Cu(21)-O(10)	114.7559	N(16)-C(15)-C(14)	121.9146	C(5)-C(4)-N(3)	118.5148
N(19)-Cu(21)-O(10)	81.0071	C(15)-C(14)-N(13)	117.6974	C(4)-N(3)-C(2)	118.7355
H(35)-N(20)-H(34)	108.6316	C(15)-C(14)-C(11)	124.0972	H(28)-C(2)-N(3)	118.012
H(35)-N(20)-Cu(22)	117.1723	N(13)-C(14)-C(11)	118.1901	H(28)-C(2)-C(1)	120.6356
H(35)-N(20)-C(15)	108.4625	C(18)-N(13)-C(14)	119.8418	N(3)-C(2)-C(1)	121.3278
H(34)-N(20)-Cu(22)	99.8601	Cu(22)-O(12)-C(11)	122.14	H(27)-C(1)-N(6)	117.6961
H(34)-N(20)-C(15)	112.5589	C(14)-C(11)-O(12)	120.358	H(27)-C(1)-C(2)	121.5398
Cu(22)-N(20)-C(15)	110.0307	C(14)-C(11)-N(9)	126.3113	N(6)-C(1)-C(2)	120.7567
H(33)-N(19)-H(32)	108.7155	O(12)-C(11)-N(9)	113.1607		
H(33)-N(19)-Cu(21)	98.3312	Cu(21)-O(10)-C(7)	125.5608		

Table S5. Bonds lengths (Å) of $[Co_2(\mathbf{APA}\text{-}2H)(H_2O)_2Cl_2]\cdot EtOH$ using DFT-method from DMOL^3 calculations.

Bond	Length (Å)	Bond	Length (Å)	Bond	Length (Å)	Bond	Length (Å)
O(26)-H(38)	1.1101	N(19)-H(32)	1.11	N(13)-C(14)	1.5122	C(4)-C(7)	1.553
O(26)-H(37)	1.11	N(19)-H(31)	1.11	O(12)-Co(22)	1.9364	C(4)-C(5)	1.5571
O(24)-H(36)	1.11	N(19)-Co(21)	1.9399	C(14)-C(11)	1.5538	N(3)-C(4)	1.5121
O(24)-H(35)	1.11	C(18)-H(30)	1.1399	C(11)-O(12)	1.5096	C(2)-H(28)	1.1401
O(24)-Co(22)	1.9502	C(17)-H(29)	1.14	O(10)-Co(21)	1.9361	C(2)-N(3)	1.5089
Cl(23)-Co(22)	2.2011	C(17)-C(18)	1.536	N(9)-C(11)	1.5101	C(1)-H(27)	1.14
O(26)-Co(21)	1.9497	N(16)-C(17)	1.5075	N(8)-N(9)	1.4791	N(6)-C(1)	1.5077
Cl(25)-Co(21)	2.2004	C(15)-N(20)	1.5119	C(7)-O(10)	1.5099	C(1)-C(2)	1.5364
N(20)-H(34)	1.1101	C(15)-N(16)	1.5114	C(7)-N(8)	1.5086		
N(20)-H(33)	1.1099	C(14)-C(15)	1.557	C(5)-N(19)	1.5121		
N(20)-Co(22)	1.9391	C(18)-N(13)	1.5087	C(5)-N(6)	1.5113		

Table S6. Bonds angles (˚) of $[Co_2(\mathbf{APA}\text{-}2H)(H_2O)_2Cl_2]\cdot EtOH$ using DFT-method from DMOL^3 calculations.

Angle	Degree (˚)	Angle	Degree (˚)	Angle	Degree (˚)
H(38)-O(26)-H(37)	109.4302	Co(22)-N(20)-C(15)	109.6599	C(14)-C(11)-N(9)	119.5847
H(38)-O(26)-Co(21)	109.2133	H(32)-N(19)-H(31)	109.4227	O(12)-C(11)-N(9)	117.9303
H(37)-O(26)-Co(21)	109.4171	H(32)-N(19)-Co(21)	109.3682	Co(21)-O(10)-C(7)	107.6198
H(36)-O(24)-H(35)	109.4408	H(32)-N(19)-C(5)	108.9992	C(11)-N(9)-N(8)	121.5672
H(36)-O(24)-Co(22)	109.4173	H(31)-N(19)-Co(21)	109.802	N(9)-N(8)-C(7)	118.5908
H(35)-O(24)-Co(22)	109.4902	H(31)-N(19)-C(5)	109.8154	O(10)-C(7)-N(8)	118.0668
O(24)-Co(22)-Cl(23)	111.0168	Co(21)-N(19)-C(5)	109.4161	O(10)-C(7)-C(4)	122.6228
O(24)-Co(22)-N(20)	111.9964	H(30)-C(18)-C(17)	120.029	N(8)-C(7)-C(4)	119.2666
O(24)-Co(22)-O(12)	112.0431	H(30)-C(18)-N(13)	120.0525	C(5)-N(6)-C(1)	120.6745
Cl(23)-Co(22)-N(20)	111.4271	C(17)-C(18)-N(13)	119.9185	N(19)-C(5)-N(6)	117.9891
Cl(23)-Co(22)-O(12)	110.4816	H(29)-C(17)-C(18)	120.0868	N(19)-C(5)-C(4)	122.2724
N(20)-Co(22)-O(12)	99.3834	H(29)-C(17)-N(16)	120.1165	N(6)-C(5)-C(4)	119.6257
O(26)-Co(21)-Cl(25)	111.2416	C(18)-C(17)-N(16)	119.7966	C(7)-C(4)-C(5)	123.4378
O(26)-Co(21)-N(19)	111.6896	C(17)-N(16)-C(15)	120.7084	C(7)-C(4)-N(3)	117.4794
O(26)-Co(21)-O(10)	110.682	N(20)-C(15)-N(16)	117.9179	C(5)-C(4)-N(3)	119.0759
Cl(25)-Co(21)-N(19)	111.7693	N(20)-C(15)-C(14)	122.3096	C(4)-N(3)-C(2)	120.8485
Cl(25)-Co(21)-O(10)	111.351	N(16)-C(15)-C(14)	119.6592	H(28)-C(2)-N(3)	120.0426
N(19)-Co(21)-O(10)	99.6008	C(15)-C(14)-N(13)	118.9783	H(28)-C(2)-C(1)	120.035
H(34)-N(20)-H(33)	109.4637	C(15)-C(14)-C(11)	123.3267	N(3)-C(2)-C(1)	119.9222
H(34)-N(20)-Co(22)	109.562	N(13)-C(14)-C(11)	117.6894	H(27)-C(1)-N(6)	120.0678
H(34)-N(20)-C(15)	109.9549	C(18)-N(13)-C(14)	120.9323	H(27)-C(1)-C(2)	120.0938
H(33)-N(20)-Co(22)	109.2137	Co(22)-O(12)-C(11)	107.1183	N(6)-C(1)-C(2)	119.8385
H(33)-N(20)-C(15)	108.9691	C(14)-C(11)-O(12)	122.4387		

Table S7. Bonds lengths (Å) of $[Pt(\mathbf{APA}\text{-}H)(H_2O)Cl_3]\cdot H_2O\cdot 2EtOH$ using DFT-method from DMOL^3 calculations.

Bond	Length (Å)	Bond	Length (Å)	Bond	Length (Å)	Bond	Length (Å)
O(23)-H(36)	1.11	N(19)-H(31)	1.1101	O(12)-Pt(21)	2.0993	C(4)-C(7)	1.5419
O(23)-H(35)	1.11	C(18)-H(30)	1.1401	C(14)-C(11)	1.5548	C(4)-C(5)	1.5449
Cl(25)-Pt(21)	2.3556	C(17)-H(29)	1.1399	C(11)-O(12)	1.5088	N(3)-C(4)	1.5104
Cl(24)-Pt(21)	2.3582	C(17)-C(18)	1.5356	N(9)-C(11)	1.5147	C(2)-H(27)	1.14
O(23)-Pt(21)	2.109	N(16)-C(17)	1.5073	N(8)-H(28)	1.1071	C(2)-N(3)	1.5094
Cl(22)-Pt(21)	2.3583	C(15)-N(20)	1.5138	N(8)-N(9)	1.4809	C(1)-H(26)	1.14
N(20)-H(34)	1.1102	C(15)-N(16)	1.512	C(7)-O(10)	1.5089	N(6)-C(1)	1.5094
N(20)-H(33)	1.1102	C(14)-C(15)	1.5575	C(7)-N(8)	1.5096	C(1)-C(2)	1.539
N(20)-Pt(21)	2.1059	C(18)-N(13)	1.508	C(5)-N(19)	1.511		
N(19)-H(32)	1.1079	N(13)-C(14)	1.5112	C(5)-N(6)	1.5111		

Table S8. Bond angles (˚) of [Pt(**APA**-H)(H_2O)Cl_3]·H_2O·2EtOH using DFT-method from DMOL^3 calculations.

Angle	Degree (˚)	Angle	Degree (˚)	Angle	Degree (˚)
H(36)-O(23)-H(35)	109.5042	H(33)-N(20)-C(15)	108.6103	O(12)-C(11)-N(9)	117.6962
H(36)-O(23)-Pt(21)	109.4916	Pt(21)-N(20)-C(15)	113.8931	C(11)-N(9)-N(8)	122.2549
H(35)-O(23)-Pt(21)	109.4627	H(32)-N(19)-H(31)	119.8452	H(28)-N(8)-N(9)	120.5454
Cl(25)-Pt(21)-Cl(24)	89.944	H(32)-N(19)-C(5)	120.3349	H(28)-N(8)-C(7)	119.7174
Cl(25)-Pt(21)-O(23)	89.9361	H(31)-N(19)-C(5)	119.8198	N(9)-N(8)-C(7)	119.7369
Cl(25)-Pt(21)-Cl(22)	89.5533	H(30)-C(18)-C(17)	120.0703	O(10)-C(7)-N(8)	119.6681
Cl(25)-Pt(21)-N(20)	179.3994	H(30)-C(18)-N(13)	120.0682	O(10)-C(7)-C(4)	120.7759
Cl(25)-Pt(21)-O(12)	90.3169	C(17)-C(18)-N(13)	119.8615	N(8)-C(7)-C(4)	119.556
Cl(24)-Pt(21)-O(23)	89.7542	H(29)-C(17)-C(18)	120.1036	C(5)-N(6)-C(1)	120.2071
Cl(24)-Pt(21)-Cl(22)	179.2842	H(29)-C(17)-N(16)	120.1069	N(19)-C(5)-N(6)	119.3033
Cl(24)-Pt(21)-N(20)	90.2003	C(18)-C(17)-N(16)	119.7893	N(19)-C(5)-C(4)	120.859
Cl(24)-Pt(21)-O(12)	90.071	C(17)-N(16)-C(15)	120.7419	N(6)-C(5)-C(4)	119.8377
O(23)-Pt(21)-Cl(22)	89.7357	N(20)-C(15)-N(16)	117.5192	C(7)-C(4)-C(5)	121.072
O(23)-Pt(21)-N(20)	90.6476	N(20)-C(15)-C(14)	122.7561	C(7)-C(4)-N(3)	119.1444
O(23)-Pt(21)-O(12)	179.6923	N(16)-C(15)-C(14)	119.6207	C(5)-C(4)-N(3)	119.7832
Cl(22)-Pt(21)-N(20)	90.3076	C(15)-C(14)-N(13)	118.9046	C(4)-N(3)-C(2)	120.233
Cl(22)-Pt(21)-O(12)	90.4413	C(15)-C(14)-C(11)	122.9298	H(27)-C(2)-N(3)	120.005
N(20)-Pt(21)-O(12)	89.0999	N(13)-C(14)-C(11)	118.1577	H(27)-C(2)-C(1)	120.0077
H(34)-N(20)-H(33)	108.6236	C(18)-N(13)-C(14)	121.0771	N(3)-C(2)-C(1)	119.9873
H(34)-N(20)-Pt(21)	108.5445	Pt(21)-O(12)-C(11)	109.3031	H(26)-C(1)-N(6)	120.0192
H(34)-N(20)-C(15)	108.4817	C(14)-C(11)-O(12)	121.8095	H(26)-C(1)-C(2)	120.0312
H(33)-N(20)-Pt(21)	108.5761	C(14)-C(11)-N(9)	120.4931	N(6)-C(1)-C(2)	119.9495

Table S9. Bond lengths (Å) of [Pd(**APA**-H)(H_2O)Cl]·$(EtOH)_{1/2}$ using DFT-method from DMOL^3 calculations.

Bond	Length (Å)	Bond	Length (Å)	Bond	Length (Å)	Bond	Length (Å)
O(22)-H(34)	1.1099	C(18)-H(28)	1.14	O(12)-Pd(21)	2.087	C(5)-N(6)	1.5108
O(22)-H(33)	1.11	C(17)-H(27)	1.1399	C(14)-C(11)	1.5573	C(4)-C(7)	1.5418
Cl(23)-Pd(21)	2.3458	C(17)-C(18)	1.5354	C(11)-O(12)	1.5099	C(4)-C(5)	1.5446
O(22)-Pd(21)	2.0975	N(16)-C(17)	1.5069	N(9)-C(11)	1.5149	N(3)-C(4)	1.5108
N(20)-H(32)	1.1101	C(15)-N(20)	1.5106	N(8)-H(26)	1.1067	C(2)-H(25)	1.1401
N(20)-H(31)	1.11	C(15)-N(16)	1.5116	N(8)-N(9)	1.4808	C(2)-N(3)	1.5091
N(20)-Pd(21)	2.0895	C(14)-C(15)	1.5571	C(7)-O(10)	1.5092	C(1)-H(24)	1.14
N(19)-H(30)	1.1079	C(18)-N(13)	1.5082	C(7)-N(8)	1.5095	N(6)-C(1)	1.5095
N(19)-H(29)	1.11	N(13)-C(14)	1.5106	C(5)-N(19)	1.5108	C(1)-C(2)	1.539

Table S10. Bonds angles (˚) of [Pd(**APA**)(H_2O)Cl]·1/2EtOH using DFT-method from DMOL^3 calculations.

Angle	Degree (˚)	Angle	Degree (˚)	Angle	Degree (˚)
H(34)-O(22)-Pd(21)	109.4642	C(17)-C(18)-N(13)	119.9035	N(9)-N(8)-C(7)	119.82
H(33)-O(22)-Pd(21)	109.613	H(27)-C(17)-C(18)	120.1288	O(10)-C(7)-N(8)	119.7379
Cl(23)-Pd(21)-O(22)	89.8849	H(27)-C(17)-N(16)	120.1279	O(10)-C(7)-C(4)	120.8417
Cl(23)-Pd(21)-N(20)	179.3931	C(18)-C(17)-N(16)	119.7434	N(8)-C(7)-C(4)	119.4171
Cl(23)-Pd(21)-O(12)	90.4317	C(17)-N(16)-C(15)	120.6591	C(5)-N(6)-C(1)	120.1962
O(22)-Pd(21)-N(20)	90.7193	N(20)-C(15)-N(16)	117.897	N(19)-C(5)-N(6)	119.3221
O(22)-Pd(21)-O(12)	179.545	N(20)-C(15)-C(14)	122.1352	N(19)-C(5)-C(4)	120.8546
N(20)-Pd(21)-O(12)	88.9638	N(16)-C(15)-C(14)	119.8389	N(6)-C(5)-C(4)	119.8231
H(32)-N(20)-H(31)	109.7835	C(15)-C(14)-N(13)	118.7078	C(7)-C(4)-C(5)	121.1058
H(32)-N(20)-Pd(21)	109.6259	C(15)-C(14)-C(11)	123.0671	C(7)-C(4)-N(3)	119.0913
H(32)-N(20)-C(15)	109.8928	N(13)-C(14)-C(11)	118.2251	C(5)-C(4)-N(3)	119.8015
H(31)-N(20)-Pd(21)	109.7371	C(18)-N(13)-C(14)	121.1457	C(4)-N(3)-C(2)	120.2436
H(31)-N(20)-C(15)	109.7275	Pd(21)-O(12)-C(11)	107.612	H(25)-C(2)-N(3)	120.0226
Pd(21)-N(20)-C(15)	108.0494	C(14)-C(11)-O(12)	121.8715	H(25)-C(2)-C(1)	120.0318
H(30)-N(19)-H(29)	119.8485	C(14)-C(11)-N(9)	120.5024	N(3)-C(2)-C(1)	119.9452
H(30)-N(19)-C(5)	120.3039	O(12)-C(11)-N(9)	117.5862	H(24)-C(1)-N(6)	120.0049
H(29)-N(19)-C(5)	119.8476	C(11)-N(9)-N(8)	122.2534	H(24)-C(1)-C(2)	120.0056
H(28)-C(18)-C(17)	120.0458	H(26)-N(8)-N(9)	120.5353	N(6)-C(1)-C(2)	119.9892
H(34)-O(22)-Pd(21)	109.4642	C(17)-C(18)-N(13)	119.9035	N(9)-N(8)-C(7)	119.82

Table S11. Decomposition steps with the temperature range and weight loss for Cu^{2+} complex of **APA**.

Compound	Decomp. Step	Temperature Range (˚C)	Remove Species	Wt. Loss	
				% (Calcd.)	% Found
[Cu_2(**APA**-H)(H_2O)Cl_3]·H_2O	1st	32 - 102	−(H_2O)	3.3	3.3
	2nd	102 - 246	−($C_4H_4N_3$ + Cl + H_2O)	27.2	27.1
	3rd	247 - 336	−($C_4H_3N_3$)	17.2	17.1
	4th	336 - 416	−(2HCl)	13.4	14.1
	5th	417 - 569	−(N_2 + C)	7.4	7.3
	residue	====	[$Cu_2(O)_2$] + C	31.5	31.1